Talin regulates moesin–NHE-1 recruitment to invadopodia and promotes mammary tumor metastasis

Brian T. Beaty,[1] Yarong Wang,[1] Jose Javier Bravo-Cordero,[1,2] Ved P. Sharma,[1,2] Veronika Miskolci,[1] Louis Hodgson,[1,2] and John Condeelis[1,2]

[1]Department of Anatomy and Structural Biology and [2]Gruss Lipper Biophotonics Center, Albert Einstein College of Medicine of Yeshiva University, Bronx, NY 10461

Invadopodia are actin-rich protrusions that degrade the extracellular matrix and are required for stromal invasion, intravasation, and metastasis. The role of the focal adhesion protein talin in regulating these structures is not known. Here, we demonstrate that talin is required for invadopodial matrix degradation and three-dimensional extracellular matrix invasion in metastatic breast cancer cells. The sodium/hydrogen exchanger 1 (NHE-1) is linked to the cytoskeleton by ezrin/radixin/moesin family proteins and is known to regulate invadopodium-mediated matrix degradation. We show that the talin C terminus binds directly to the moesin band 4.1 ERM (FERM) domain to recruit a moesin–NHE-1 complex to invadopodia. Silencing talin resulted in a decrease in cytosolic pH at invadopodia and blocked cofilin-dependent actin polymerization, leading to impaired invadopodium stability and matrix degradation. Furthermore, talin is required for mammary tumor cell motility, intravasation, and spontaneous lung metastasis in vivo. Thus, our findings provide a novel understanding of how intracellular pH is regulated and a molecular mechanism by which talin enhances tumor cell invasion and metastasis.

Introduction

Tumor cell metastasis is a multistep process that involves invasion through the stroma, intravasation, extravasation, and colonization of secondary sites (Steeg, 2003; Madsen and Sahai, 2010; Valastyan and Weinberg, 2011). Invadopodia are actin-rich protrusions that are formed by metastatic tumor cells to degrade the ECM and facilitate the invasive stages of metastasis (Yamaguchi et al., 2005; Eckert et al., 2011; Huttenlocher and Horwitz, 2011). Invadopodia initially form as precursor structures, which are enriched in actin regulators, including cortactin, N-WASp, Arp2/3, cofilin, fascin, and others, but are not yet capable of degrading the ECM (Artym et al., 2006; Oser et al., 2009; Li et al., 2010). The sodium/hydrogen exchanger 1 (NHE-1) is then recruited to invadopodium precursors to drive cofilin-dependent actin polymerization and matrix protease recruitment (e.g., MT1-MMP) for ECM degradation (Artym et al., 2006; Sakurai-Yageta et al., 2008; Magalhaes et al., 2011).

Although NHE-1 plays a critical role in regulating invadopodium function by modulating intracellular pH (Busco et al., 2010; Lucien et al., 2011; Magalhaes et al., 2011; Brisson et al., 2013), the proteins that regulate its recruitment and activity at invadopodia remain poorly understood. In fibroblasts, NHE-1 is linked to the cytoskeleton by ezrin/radixin/moesin (ERM) proteins, and it interacts with multiple adhesion proteins including α5β1 integrin, talin, and FAK to regulate cell adhesion and migration (Schwartz et al., 1991; Srivastava et al., 2008; Choi et al., 2013). As several groups have recently shown that focal adhesion proteins (e.g., β1 integrin, FAK, paxillin, and Hic-5) regulate invadopodial maturation (Nakahara et al., 1998; Mueller et al., 1999; Chan et al., 2009; Linder et al., 2011; Branch et al., 2012; Pignatelli et al., 2012b; Beaty et al., 2013), we investigated whether the focal adhesion protein talin might recruit NHE-1 to invadopodia.

Talin is a large, band 4.1 ERM (FERM) family protein that has been shown to play a critical role in structurally linking integrins to the actin cytoskeleton, stimulating "inside-out" integrin activation and regulating focal adhesion turnover (Jiang et al.,

Correspondence to Brian Beaty: brian.beaty@med.einstein.yu.edu; or John Condeelis: john.condeelis@einstein.yu.edu

Abbreviations used in this paper: BCECF, 2′,7′-bis (2-carboxyethyl), 5 (and -6) carboxyfluorescein; DD, dimerization domain; ERM, ezrin/radixin/moesin; FERM, band 4.1 ERM; KVK/D, K2443D/V2444D/K2445D; NHE-1, sodium/hydrogen exchanger 1; TIRF, total internal reflection fluorescence microscope; WT, wild type.

The Rockefeller University Press $30.00
J. Cell Biol. Vol. 205 No. 5 737–751
www.jcb.org/cgi/doi/10.1083/jcb.201312046

2003; Tadokoro et al., 2003; Tanentzapf and Brown, 2006; Srivastava et al., 2008; Huang et al., 2009). Talin is reported to be present in membrane protrusion fractions isolated from transformed chicken embryo fibroblasts, suggesting that it may also be enriched in invadopodia in tumor cells (Mueller et al., 1992). Here, we evaluate the role of talin in regulating invadopodium function as well as tumor cell metastasis in vivo and explore the mechanism by which NHE-1 is recruited to invadopodia.

Results

Talin stabilizes invadopodia to promote matrix degradation

To investigate the role of talin in regulating invadopodial function, we used the highly metastatic human breast carcinoma cell line MDA-MB-231, which has been shown to form invadopodia in vitro and spontaneously metastasize in mice (Artym et al., 2006; Patsialou et al., 2009). To quantify invadopodium formation and matrix degradation, cells were plated on Alexa Fluor 405–labeled gelatin for 4 h before fixation and stained with invadopodial markers cortactin and Tks5. We found that talin localizes to the invadopodium core (protrusion) in MDA-MB-231 cells (Fig. 1 A). To determine when talin is enriched at invadopodia, cells were stimulated with EGF to induce the formation of nondegradative invadopodium precursors (Oser et al., 2010; Yamaguchi et al., 2011). Talin becomes significantly enriched at the core of precursors between 3 and 5 min of EGF stimulation, which coincides with the actin polymerization step of invadopodial maturation (Fig. S1, A and B; $P < 0.036$; Oser et al., 2009).

Next, we used siRNA directed against talin to selectively deplete the protein by ∼90–95% in MDA-MB-231 cells compared with those transfected with control, nontargeting siRNA (Fig. 1 B). Mean cell area (spreading) is only slightly reduced and focal adhesion formation is not affected on gelatin, similar to what has been previously observed in mammary epithelial cells (Fig. S2; Wang et al., 2011). To evaluate whether talin knockdown affects invadopodium function, cells were plated on 405-labeled gelatin. Talin-depleted cells have an ∼7-fold reduction in the number of mature (matrix-degrading) invadopodia and an ∼3.6-fold reduction in the degradation area per cell relative to control cells (Fig. 1, C–E). To confirm this finding in another cell line, talin was stably knocked down in rat mammary adenocarcinoma MTLn3 cells using shRNA and similar results were obtained (Fig. S3, A and B).

Invadopodia initially form as nondegradative invadopodium precursors that subsequently undergo actin polymerization and recruit matrix proteases to develop into mature, matrix-degrading invadopodia. To test whether talin is required for the initial formation of invadopodium precursors, the EGF stimulation assay was used. Interestingly, the number of invadopodium precursors formed in response to EGF is nearly identical in control and talin siRNA-treated cells (Fig. 1 F). Once invadopodium precursors form, the structure is stabilized by Tks5–PI(3,4)P_2 interactions, β1 integrin–mediated adhesion, and ongoing actin polymerization (Yamaguchi et al., 2005, 2011; Beaty et al., 2013; Sharma et al., 2013a). Because talin affects invadopodium maturation, we hypothesized that it may be involved in stabilizing invadopodia for subsequent matrix degradation. Invadopodium stability was evaluated by measuring the mean lifetime of TagRFP-cortactin– and GFP-Tks5–rich invadopodia in control and talin knockdown cells using time-lapse microscopy. We found that the lifetimes of both invadopodium precursors and mature invadopodia are significantly reduced in talin-depleted cells (Fig. 1 G and Videos 1 and 2; $P < 0.00013$). Together, these data show that talin plays a role in the stabilization and maturation of invadopodia, rather than the initial formation of invadopodium precursors.

The C-terminal actin binding site is necessary for talin localization and invadopodium maturation

Talin consists of two domains: a globular head domain and an elongated rod domain (Burridge and Connell, 1983; Molony et al., 1987; Gingras et al., 2008; Goksoy et al., 2008; Anthis et al., 2009; Elliott et al., 2010; Kim et al., 2012). The head domain activates integrins and contains binding sites for β integrin cytoplasmic tails, PI(4,5)P_2, FAK, and actin, whereas the rod domain contains multiple binding sites for vinculin, as well as two more actin binding sites and a second integrin binding site (Burridge and Mangeat, 1984; Horwitz et al., 1986; Nuckolls et al., 1990; McLachlan et al., 1994; Hemmings et al., 1996; Xing et al., 2001; Goksoy et al., 2008; Gingras et al., 2009; Calderwood et al., 2013). To better understand whether the head or rod domain is required for talin recruitment to invadopodia, endogenous talin was knocked down using siRNA, and wild-type (WT) GFP-talin, GFP–talin head domain, or GFP–talin rod domain was expressed to a similar level (Fig. S1 C; Franco et al., 2004; Simonson et al., 2006; Wang et al., 2011). Although WT GFP-talin and the GFP–talin rod domain are significantly enriched in invadopodia by ∼40–50% over background cytosolic levels, the talin head domain does not localize to invadopodia above background (Fig. 2, A and B).

To further characterize the mechanism of talin recruitment to invadopodia, interactions with β1 integrin and actin were evaluated because both localize to the invadopodium core and bind to the talin rod domain (β3 integrin does not localize to invadopodia; Franco et al., 2006; Moes et al., 2007; Gingras et al., 2008, 2009, 2010; Ellis et al., 2011; Beaty et al., 2013). Surprisingly, when the α-helical structure of the integrin binding site in the R11 talin rod domain is mutated (L2094A/I2095A; LI/A), talin recruitment to invadopodia is unaffected (Fig. 2, A and B; Moes et al., 2007; Ellis et al., 2011; Wang et al., 2011; Goult et al., 2013). To confirm this finding, β1 integrin was depleted in MDA-MB-231 cells using siRNA, and talin enrichment at invadopodia was measured. Consistent with the mutant data, talin is recruited to invadopodium precursors in β1 integrin knockdown cells as efficiently as in control cells (Fig. S4, A and F). Introduction of a K2443D/V2444D/K2445D (KVK/D) mutation into the C-terminal actin binding site of talin (R13 domain) has been shown to significantly inhibit talin binding to actin (Gingras et al., 2008). To determine whether this binding event plays a role in talin recruitment to invadopodia, GFP–talin rod–KVK/D was expressed in MDA-MB-231 cells. Results indicate that this mutation significantly impairs talin localization to invadopodia (Fig. 2, A

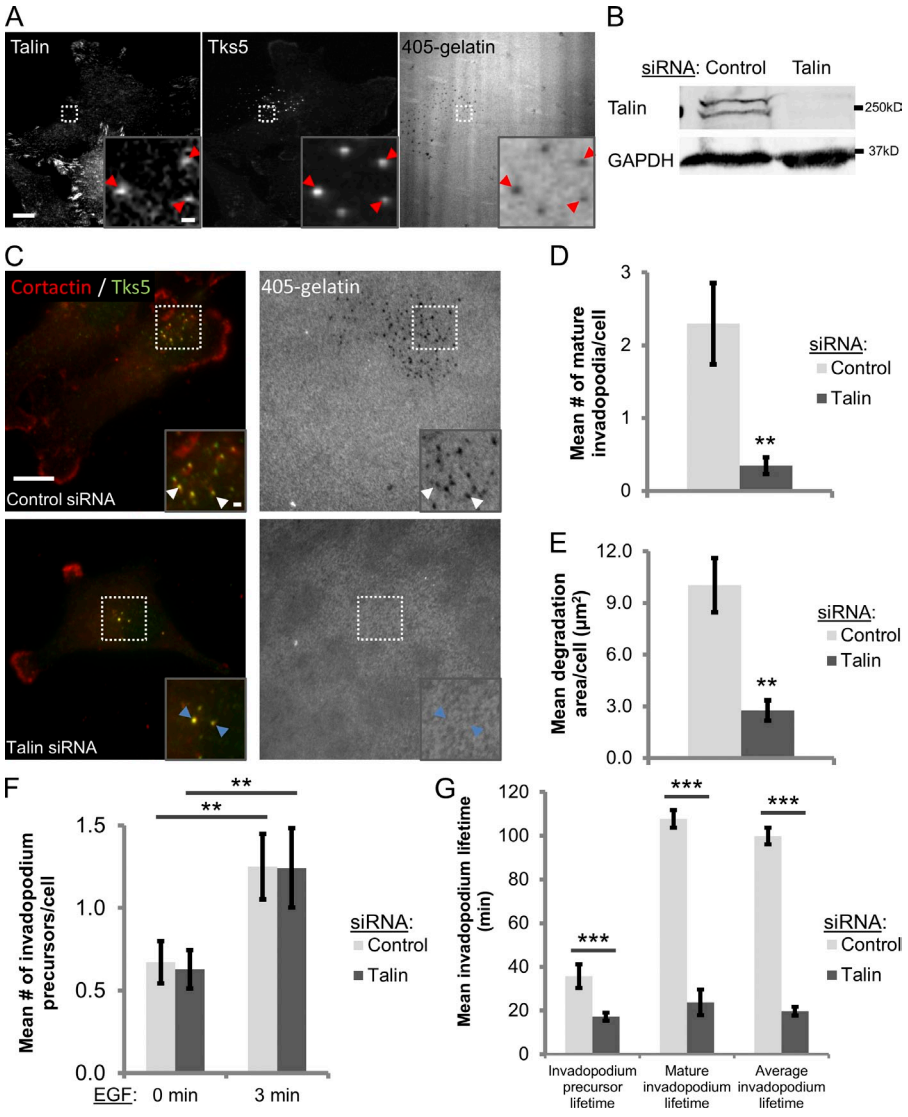

Figure 1. **Talin localizes to invadopodia and is required for their stabilization and maturation.** (A) Talin localizes to the invadopodium core in MDA-MB-231 cells plated on Alexa Fluor 405–labeled gelatin for 4 h. Representative confocal images of talin and Tks5 staining. Red arrowheads denote mature invadopodia with colocalization of talin and Tks5 in the invadopodium core. Inset shows magnified image of invadopodia in the box. Bars: (main panel) 10 µm; (inset) 1 µm. (B) Western blot analysis of MDA-MB-231 cells transfected with control or talin1 siRNA (SMARTpool) for 96 h. Blots were stained for talin and GAPDH (loading control). (C–E) Steady-state invadopodial matrix degradation assay. (C) Representative images of MDA-MB-231 cells stained for cortactin and Tks5. White arrowheads denote mature invadopodia; blue arrowheads denote invadopodium precursors. Inset shows magnified image of invadopodia in the box. Bars: (main panel) 10 µm; (inset) 1 µm. (D) Quantification of the number of mature invadopodia per cell. Mature invadopodia are defined as cortactin-/Tks5-rich punctate structures colocalized with a matrix degradation hole. $n > 52$ cells; three independent experiments. **, $P < 0.0076$. (E) Quantification of invadopodial matrix degradation area per cell. $n > 52$ cells; three independent experiments. **, $P = 0.0017$. (F) EGF stimulation assay. Quantification of the number of invadopodium precursors in MDA-MB-231 cells stimulated with 2.5 nM EGF for 0 (unstimulated) or 3 min. Precursors are defined as cortactin-/F-actin–rich punctate structures that do not colocalize with a matrix degradation hole. $n > 58$ cells; three independent experiments. **, $P < 0.018$. (G) Quantification of invadopodium precursor, mature invadopodium, and mean (pooled) invadopodium lifetimes in MDA-MB-231 cells treated with control or talin siRNA and transfected with TagRFP-cortactin and GFP-Tks5 plated on 405-labeled gelatin. Cells were imaged for 3 h using time lapse microscopy (see Videos 1 and 2). $n > 46$ precursors; $n > 28$ mature invadopodia; three independent experiments. ***, $P < 0.00013$. Error bars represent the SEM.

and B; $P < 0.0019$). Hence, talin binding to actin, not β1 integrin, is required for its localization to invadopodia.

Next, we asked whether the talin head and rod domains as well as integrin and actin binding were required for invadopodial maturation. MDA-MB-231 cells were again treated with either control or talin siRNA and transfected with GFP (vector control) or one of the GFP-tagged talin constructs. As expected, control GFP cells form significantly more mature invadopodia than talin knockdown GFP cells, which are essentially unable to form mature invadopodia (Fig. 2, A and C; $P = 0.0034$). Consistent with the localization experiments, both WT GFP-talin and the GFP–talin rod domain rescue the invadopodium maturation defect, producing similar numbers of mature invadopodia as control GFP cells (Fig. 2). The GFP–talin head domain and GFP–talin rod–KVK/D constructs are unable to rescue invadopodium maturation, and these cells form significantly fewer invadopodia than the control, WT, and talin rod–expressing cells (Fig. 2, A and C; $P < 0.048$). Interestingly, despite localizing normally to invadopodia, the talin rod–LI/A mutant does not rescue invadopodium maturation (Fig. 2). Together, these results indicate that the C-terminal portion of the talin rod domain (R11–13) is critical for talin-mediated invadopodial maturation, and the talin head domain does not regulate invadopodium function.

The talin rod domain is required for NHE-1 localization to invadopodia

NHE-1 increases pH_i to affect the function of numerous cytoskeletal proteins in lamellipodia as well as invadopodia (Denker et al., 2000; Frantz et al., 2008; Srivastava et al., 2008; Busco et al., 2010; Magalhaes et al., 2011). An important step in invadopodium maturation is the regulation of pH_i by NHE-1 (Busco et al., 2010; Magalhaes et al., 2011). Given that talin enhances invadopodium stability and maturation, we hypothesized that talin may modulate the actin polymerization step in invadopodial maturation, specifically by regulating NHE-1 (Magalhaes et al., 2011). Coimmunoprecipitation showed that endogenous talin indeed forms a complex with NHE-1 in MDA-MB-231 cell lysates (Fig. 3 A). Because the mechanism of NHE-1 recruitment to invadopodia is not known, we evaluated whether talin may be important for this step. To this end, knockdown rescue experiments

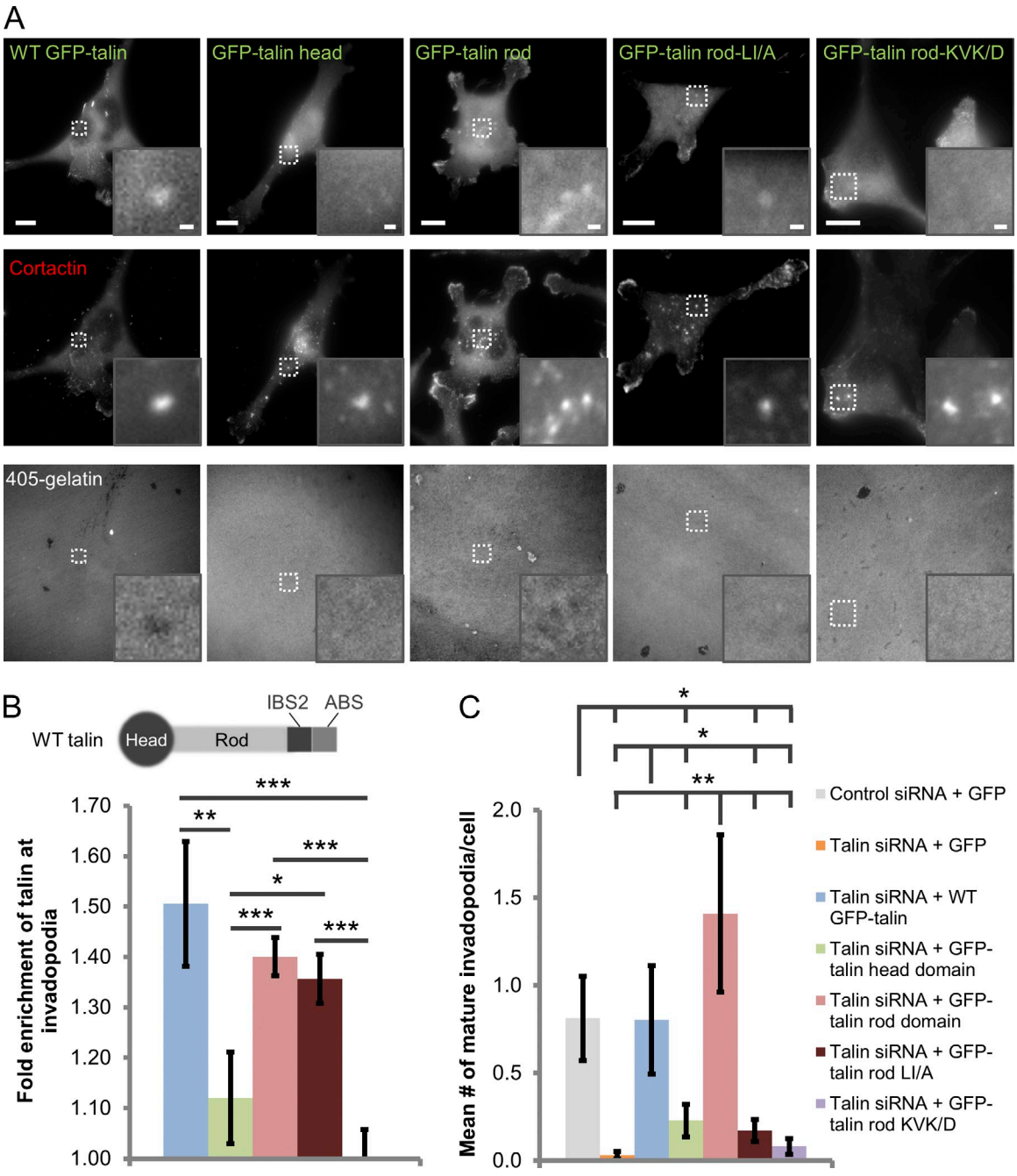

Figure 2. **The actin binding site in the talin rod domain is required for talin localization to invadopodia and matrix degradation.** (A) Representative images of MDA-MB-231 cells plated on 405-labeled gelatin, showing that WT GFP-talin, the GFP–talin rod domain, and the talin rod-LI/A mutant localize to the cortactin-rich invadopodium core. Inset shows magnified image of invadopodia in the box. Bars: (main panel) 10 µm; (inset) 1 µm. (B) Quantification of talin enrichment at invadopodia relative to cytosolic levels in talin siRNA-treated cells expressing GFP-tagged talin constructs. $n > 33$ invadopodia; three independent experiments. *, P = 0.032; **, P = 0.015; ***, P < 0.0019. Cartoon depicting the domain structure of talin is shown, including the C-terminal integrin binding site 2 (IBS2) and actin binding site (ABS). (C) Quantification of the number of mature invadopodia per cell in cells treated with either control or talin siRNA and transfected with GFP or GFP-tagged talin constructs. $n > 41$ cells; three independent experiments. *, P < 0.048; **, P = 0.0093. Error bars represent the SEM.

were performed. NHE-1 is enriched in the invadopodium core in control GFP cells by ∼34% above cytosolic levels (Fig. 3, B and C). In talin-depleted GFP cells, however, NHE-1 levels at invadopodium precursors are significantly reduced and remain similar to the surrounding cytosol (Fig. 3, B and C; P = 0.022). Consistent with the invadopodium maturation data, WT GFP-talin and GFP–talin rod domain are able to rescue NHE-1 recruitment to invadopodia, but the talin head domain and the LI/A and KVK/D talin mutants cannot (Fig. 3 C).

To assay NHE-1 function at invadopodia, we used the pH-sensitive dye 2′,7′-bis (2-carboxyethyl), 5 (and -6) carboxyfluorescein (BCECF; Frantz et al., 2008). Although the pH_i at invadopodia of control cells is ∼7.05, it is significantly reduced in talin knockdown cells (pH of ∼6.8; Fig. 3 D; P = 0.012),

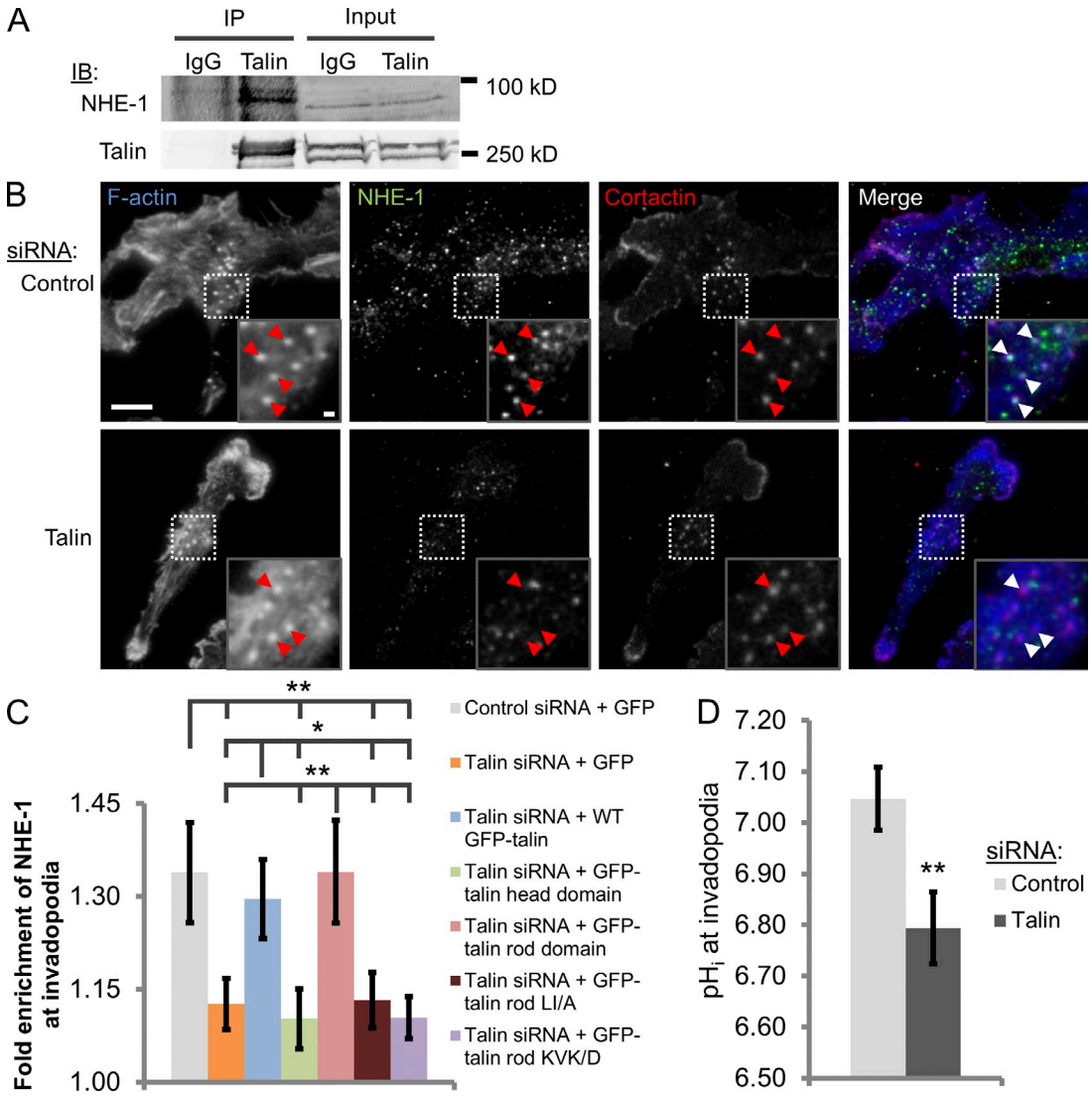

Figure 3. **Talin recruits NHE-1 to invadopodia and promotes NHE-1–dependent alkalinization of the intracellular space at invadopodia.** (A) Coimmunoprecipitation of NHE-1 with talin. Cells were starved for 16 h and stimulated with 2.5 nM EGF. Endogenous talin was immunoprecipitated from MDA-MB-231 cell lysates using the 8d4 talin antibody, and the resulting immunoprecipitates were subjected to Western blotting with anti–NHE-1 and talin antibodies. IgG served as a negative control; three independent experiments. (B and C) Talin regulates NHE-1 localization to invadopodia. (B) MDA-MB-231 cells were stained with phalloidin (F-actin), NHE-1, and cortactin. Inset shows magnified image of invadopodia in the box. Red arrowheads denote invadopodia. Bars: (main panel) 10 µm; (inset) 1 µm. (C) Quantification of NHE-1 enrichment at invadopodia in control and talin siRNA-treated cells transfected with GFP or a series of GFP-tagged talin constructs. $n > 47$ invadopodia; three independent experiments. *, $P = 0.034$; **, $P < 0.029$. (D) Quantification of mean intracellular pH at invadopodia (BCECF pH biosensor). $n > 56$ invadopodia; three independent experiments. **, $P = 0.012$. Error bars represent the SEM.

similar to levels observed in NHE-1–depleted cells (Magalhaes et al., 2011), indicating that NHE-1 activity is diminished and hydrogen ions accumulate in the intracellular space at invadopodia. Collectively, these data demonstrate that the C-terminal portion of the talin rod domain is essential for NHE-1 recruitment to invadopodia, and talin is an important upstream regulator of NHE-mediated modulation of pH_i at invadopodia.

Talin binds directly to moesin in vitro and recruits a moesin–NHE-1 complex to invadopodia

We have previously shown that when the ERM binding site in NHE-1 is mutated, its localization to invadopodia is impaired, and phosphorylated ERM proteins have recently been shown to coimmunoprecipitate with NHE-1 in ventral structures (Magalhaes et al., 2011; Antelmi et al., 2013). Moesin is an ERM protein that is uniquely up-regulated in invasive subpopulations of MDA-MB-231 cells in vivo (ezrin and radixin expression are unchanged) and is also up-regulated in invasive melanoma cells in which it promotes 3D matrix invasion (Estecha et al., 2009; Patsialou et al., 2012). Here, we show that moesin and pan-phospho-ERM proteins, but not ezrin or radixin, localize to invadopodia in MDA-MB-231 cells and that moesin is required for NHE-1 localization to invadopodia (Fig. 4 A and S4, B–E). To determine if moesin or ezrin regulates invadopodium maturation, we selectively knocked them down using siRNA and plated cells on 405-labeled gelatin (Fig. 4 B and S4 G). Moesin-depleted cells form significantly fewer mature invadopodia compared with control

cells, whereas ezrin knockdown has no effect on invadopodia (Fig. 4 C; P = 0.017). Thus, we show that moesin promotes invadopodium maturation by recruiting NHE-1.

Because both talin and moesin are required for NHE-1 localization to invadopodia, we hypothesized that talin may recruit moesin in complex with NHE-1 (Magalhaes et al., 2011). In support of this, we found that endogenous talin coimmunoprecipitates with moesin, but not ezrin, in MDA-MB-231 cell lysates (Fig. 4 D). To determine if talin binds directly to moesin, we purified recombinant His-tagged talin and GST-tagged moesin as described previously (Calderwood et al., 1999; Gonzalez-Agosti et al., 1999; Xing et al., 2001; Bakolitsa et al., 2004). Full-length, N-terminal (amino acids 1–322; moesin-N), and C-terminal GST-moesin fragments (amino acids 307–577; moesin-C) were fused to glutathione agarose beads for in vitro binding assays (Bravo-Cordero et al., 2013). To map the moesin binding site on talin, the following recombinant talin fragments were generated: talin head domain, talin rod R1–5 domains, talin rod R6–10 domains, and talin rod R11–dimerization domain (DD; Goult et al., 2013).

The talin head, rod R1–5, and rod R6–10 domains do not bind any of the moesin proteins; however, the C-terminal talin rod R11-DD binds strongly to full-length moesin and moesin-N, with lower affinity for moesin-C (Figs. 4 F and S5 C). To further characterize the moesin binding site on talin, talin rod R11, R12, and R13-DD domain recombinant proteins were generated. Talin R12 bound to all of the moesin constructs, whereas talin R13-DD bound primarily to full-length moesin and moesin-N and R11 weakly bound moesin-N only (Fig. 4 F). Because the LI/A and KVK/D mutations are located in the moesin binding site, we generated recombinant talin R11-DD fragments that contain the LI/A and KVK/D mutations to evaluate the effect of disrupting R11 and R13 on talin binding to moesin, respectively. We found that both of these mutations dramatically impair talin binding to moesin in vitro (Fig. S5 C). Thus, we have identified a novel direct binding interaction between talin and moesin, in which the C-terminal region of the talin rod domain (R11-DD) binds to the N-terminal FERM domain of moesin (Fig. 4 G).

To determine if talin is required for moesin localization to the invadopodium compartment, cells were treated with either control or talin siRNA and GFP or GFP-tagged talin constructs were expressed. We found that moesin is significantly enriched in invadopodia by ∼40% relative to the surrounding cytosol; however, its localization is impaired in talin knockdown cells (Fig. 4 E). Moesin recruitment to invadopodia is rescued by WT GFP-talin and GFP–talin rod domain, but not by the R11 and R13 mutants (LI/A or KVK/D, respectively), which were shown to disrupt moesin binding in vitro (Fig. 4, E and F; and Fig. S5 C). Because the LI/A mutant also affects integrin binding, β1 integrin was knocked down and moesin enrichment was quantified. Moesin localization to invadopodia is significantly impaired in β1 integrin knockdown cells (Fig. S4 A; P = 0.007). Collectively, these data indicate that β1 integrin promotes talin-mediated moesin recruitment to invadopodia via its C-terminal R11 and R13 domains.

Conversely, moesin knockdown does not affect talin localization to invadopodia, suggesting that talin is upstream of moesin in the NHE-1 pathway (Fig. S5 A). To confirm this, constitutively active moesin (T558D), a mutation that disrupts its autoinhibited conformation and enhances binding to F-actin, was expressed in control or talin siRNA-treated cells (Nakamura et al., 1995, 1999; Fehon et al., 2010; Solinet et al., 2013). Although moesin T558D induces invadopodium maturation in control cells, the number of mature invadopodia in talin KD cells GFP or moesin-GFP T558D are similar and significantly reduced relative to control cells (Fig. S5 B; P < 0.01). Together, these data demonstrate that talin is a novel moesin binding partner and functions upstream of moesin–NHE-1 to promote invadopodium maturation.

Talin is required for actin polymerization at invadopodia

Given that talin promotes invadopodium maturation by regulating NHE-1 function, we hypothesized that talin-depleted cells may have impaired actin polymerization, as this is a key step in the transformation of an invadopodium precursor into a mature, matrix-degrading invadopodium. Recent work has shown that cofilin severs F-actin to form barbed ends that are used to elongate filaments required to support dendritic nucleation by Arp2/3 (DesMarais et al., 2004; Pollard, 2007; Frantz et al., 2008; Beaty et al., 2013). During the early stages of invadopodium precursor formation, cortactin sequesters cofilin, inactivating it (Oser et al., 2009). NHE-1 disrupts this inhibitory interaction by increasing the pH_i, allowing cofilin to be released and sever actin filaments to drive actin polymerization (Magalhaes et al., 2011).

To quantify actin barbed end formation, the barbed end assay was used to measure the incorporation of biotinylated actin into actively polymerizing filaments within invadopodium precursors (Chan et al., 1998; Oser et al., 2010). A peak of barbed end formation occurs after 3 min of EGF stimulation in MDA-MB-231 cells (Oser et al., 2010). In control cells, EGF induces a significant increase in cofilin-dependent barbed end formation at invadopodium precursors, whereas EGF-stimulated barbed end formation is abrogated in talin and moesin knockdown cells (Fig. 5; $P < 2.4 \times 10^{-7}$). Similar results were observed in MTLn3 cells, suggesting that talin and moesin are necessary for the cofilin-dependent actin polymerization step in invadopodial maturation (Fig. S3 C).

Talin is essential for tumor cell invasion, intravasation, and lung metastasis

Because invadopodia promote tumor cell invasion through the stroma (Eckert et al., 2011; Huttenlocher and Horwitz, 2011; Gligorijevic et al., 2012), we hypothesized that talin would be required for tumor cells to migrate through a dense 3D ECM. To test this, an inverted 3D invasion assay was used (Caswell et al., 2007; Tuomi et al., 2009; Deakin and Turner, 2011). Cells were plated on the bottom of a transwell and stimulated to invade into 3D ECM, consisting of type I collagen and Matrigel, by a chemotactic gradient (Nyström et al., 2005; Gaggioli et al., 2007). Talin knockdown reduces 3D ECM invasion by 60% compared with control cells, indicating that talin is required for invasive cell migration in a physiologically relevant 3D ECM (Fig. 6 A).

To evaluate the role of talin in regulating mammary tumor cell motility and metastasis in vivo, MTLn3 mammary adenocarcinoma cells stably expressing either control or talin shRNA

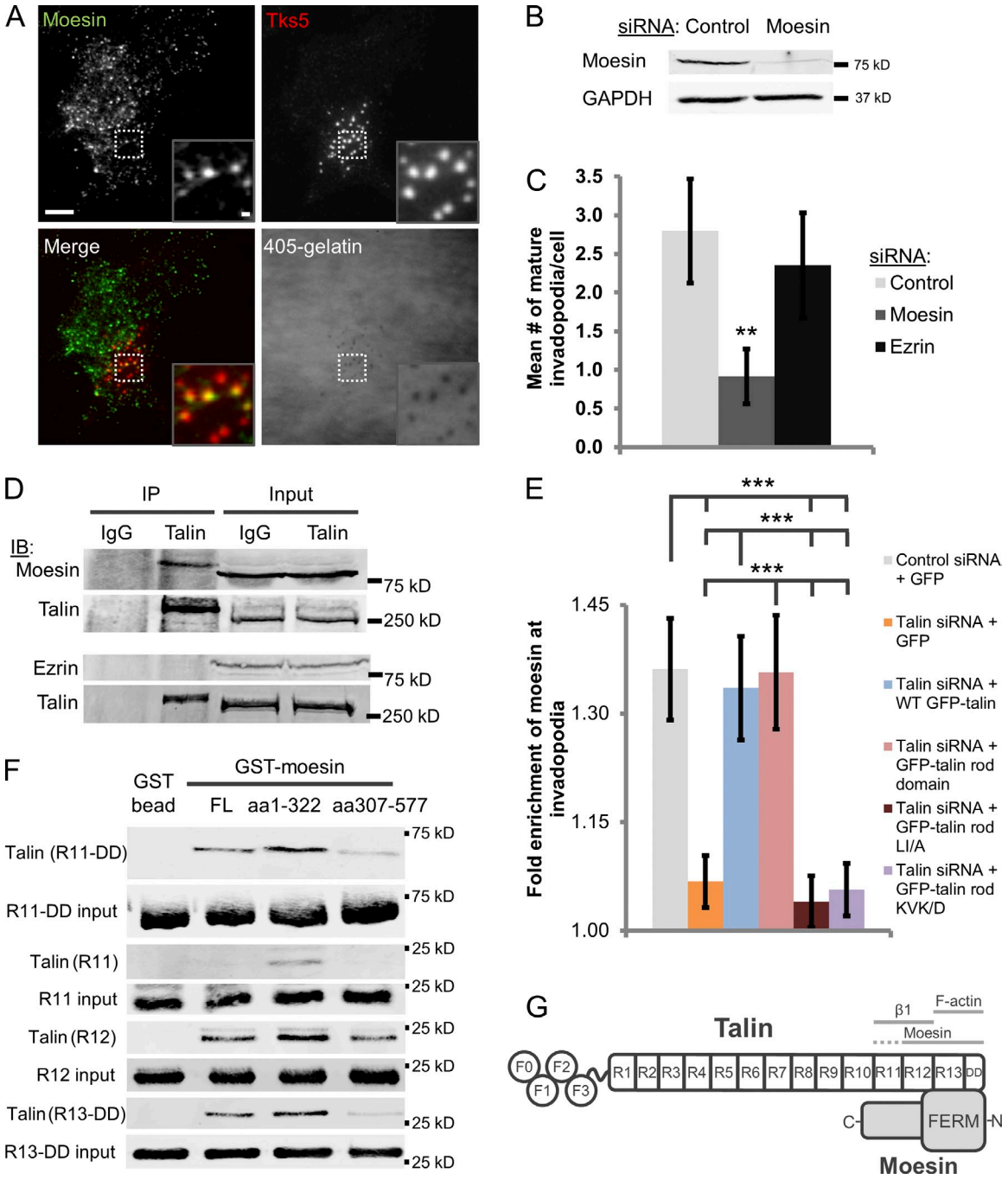

Figure 4. **Moesin localizes to invadopodia in a talin-dependent manner to promote invadopodium maturation.** (A) Moesin localizes to invadopodia. Representative TIRF images of moesin and Tks5 staining in cells plated on 405-labeled gelatin. Bars: (main panel) 10 µm; (inset) 1 µm. (B) Western blot analysis of MDA-MB-231 cells transfected with control or moesin siRNA (SMARTpool) for 72 h. Blots were stained for moesin and GAPDH (loading control). (C) Quantification of the number of mature invadopodia per cell in control and moesin- and ezrin-depleted cells. $n > 56$ cells; three independent experiments. **, $P = 0.017$. (D) Coimmunoprecipitation of moesin with talin. Cells were starved for 16 h and stimulated with 2.5 nM EGF. Endogenous talin was immunoprecipitated from MDA-MB-231 cell lysates using the 8d4 talin antibody, and the resulting immunoprecipitates were subjected to Western blotting with anti-moesin, anti-ezrin, and anti-talin antibodies. The amount of talin immunoprecipitated in each of the two experiments is shown as a control. IgG served as a negative control for the immunoprecipitation; three independent experiments. (E) Quantification of moesin enrichment at invadopodia in control and talin siRNA-treated cells and then transfected with a series of GFP-tagged talin constructs. $n > 46$ invadopodia; three independent experiments. ***, $P < 0.0023$. Error bars represent the SEM. (F) In vitro direct binding pulldown assay with His-tagged talin and GST-tagged moesin (latter fused to agarose beads). Western blots are stained for talin (TD77, R11-DD) or anti-His. Three independent experiments. (G) Schematic of the talin–moesin binding interaction. The moesin N terminus binds to talin domains R11-DD (with higher affinity for R12 and R13-DD than R11). The talin R12 domain, but not R13-DD, also binds to the moesin C terminus. Solid gray lines indicate binding sites for β1 integrin, actin, and moesin; dashed line over R11 indicates lower affinity binding.

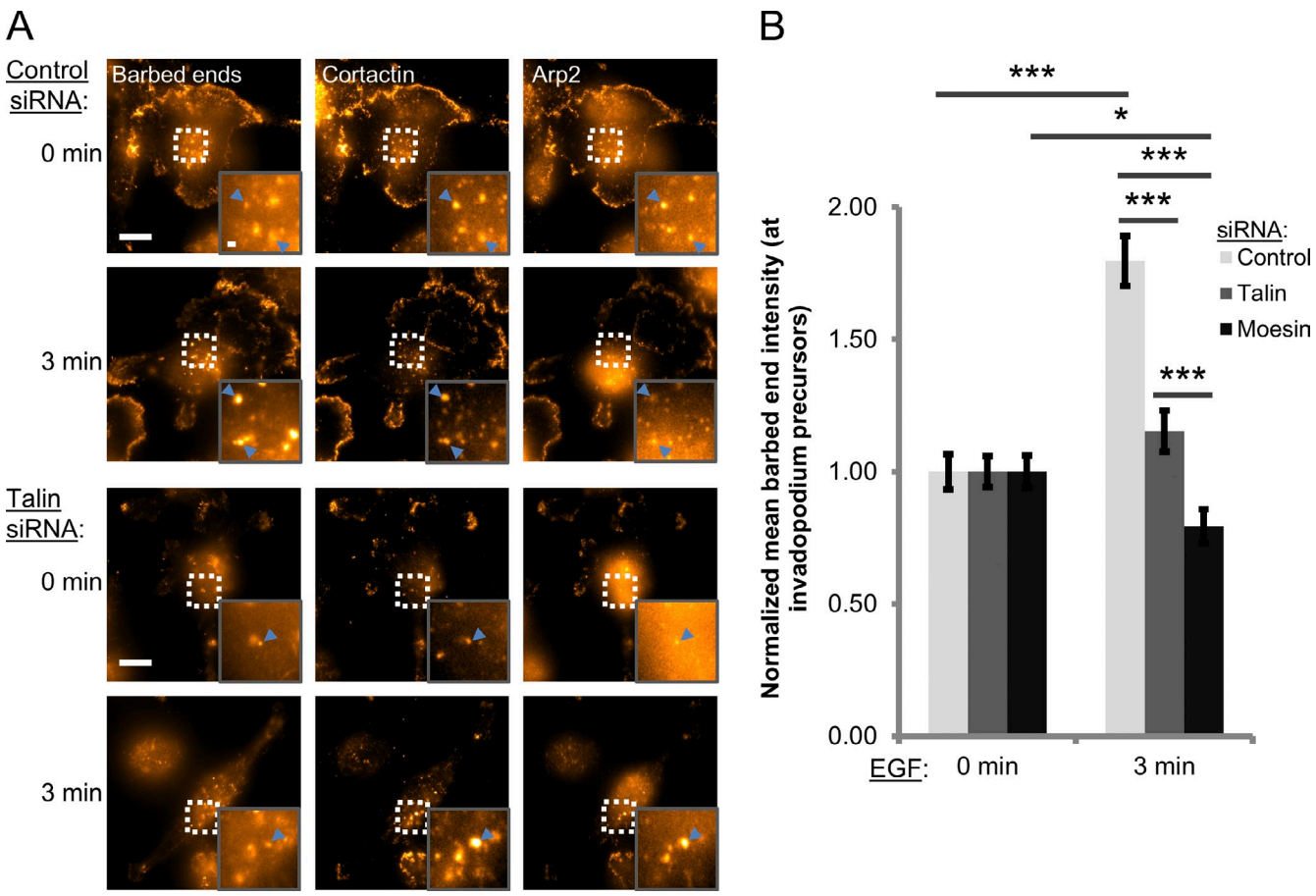

Figure 5. **Free actin barbed end formation is impaired in talin- and moesin-depleted cells.** (A and B) Barbed end formation assay. (A) Representative images of control and talin-depleted cells stained for barbed ends (anti-biotin), cortactin, and Arp2. Invadopodium precursors are defined as cortactin-/Arp2-rich punctate structures. Blue arrowheads denote invadopodium precursors. Inset shows magnified image of invadopodia in the box. Bars: (main panel) 10 µm; (inset) 1 µm. (B) Quantification of barbed end intensity within invadopodium precursors after stimulation with 2.5 nM EGF for 0 (unstimulated) or 3 min. $n > 80$ invadopodia; three independent experiments. *, $P = 0.0247$; ***, $P < 4.52 \times 10^{-4}$. Error bars represent the SEM.

and Dendra2 (to visualize tumor cells) were injected into the mammary glands of severe combined immunodeficiency mice (Fig. 6 B; Linder et al., 2011; Bravo-Cordero et al., 2012). After 4 wk, the mice were sacrificed, and the lungs and tumors were harvested. Spontaneous tumor cell dissemination to the lung was quantified by counting the number of Dendra-positive tumor cells in each lung lobe, an assay that differentiates dissemination from tumor growth at the distant site (Goldberg et al., 1999; Cameron et al., 2000; Roussos et al., 2011). Although the primary talin shRNA tumors were larger, we found that control mice have six times more metastatic tumor cells in the lung than talin shRNA mice, similar to what has been shown previously in Arg knockdown breast tumors and glioblastoma multiforme cells (Fig. S5 D and Fig. 6, C and D; Dhruv et al., 2013; Gil-Henn et al., 2013).

For tumor cells to spread to distant organs, they must migrate through the stroma and degrade the endothelial basement membrane to enter a blood vessel, both of which require invadopodium-mediated matrix degradation (Cardone et al., 2005; Eckert et al., 2011; Bravo-Cordero et al., 2012; Gligorijevic et al., 2012; Roh-Johnson et al., 2013). Intravital multiphoton imaging demonstrates that talin-depleted tumor cells have impaired protrusion formation and tumor cell motility in vivo, suggesting that these cells are unable to efficiently invade the surrounding ECM because of defects in invadopodium and possibly adhesion formation (Fig. 6 E and Videos 3 and 4; Zhang et al., 2008). To determine if the impaired lung metastasis in talin knockdown mice was caused by decreased intravasation, cardiac puncture of the right atrium was performed to evaluate the number of circulating tumor cells in the blood (Wyckoff et al., 2000; Helzer et al., 2009; Roussos et al., 2011; Patsialou et al., 2012). Mice bearing control tumors have eight times more circulating tumor cells than those with talin shRNA tumors (Fig. 6 F). Collectively, these results indicate that talin promotes tumor cell protrusion formation, motility, and intravasation into the blood, leading to enhanced metastasis to the lung.

Discussion

In this study, we describe a novel signaling axis involving talin, moesin, and NHE-1. Although talin is dispensable for the initial stages of invadopodium precursor formation, it plays a critical role in invadopodium stabilization and matrix degradation. The talin R12 and R13-DD domains (and R11 to a lesser extent) bind directly to the moesin FERM domain in vitro, and these domains are required for moesin–NHE-1 recruitment and invadopodium

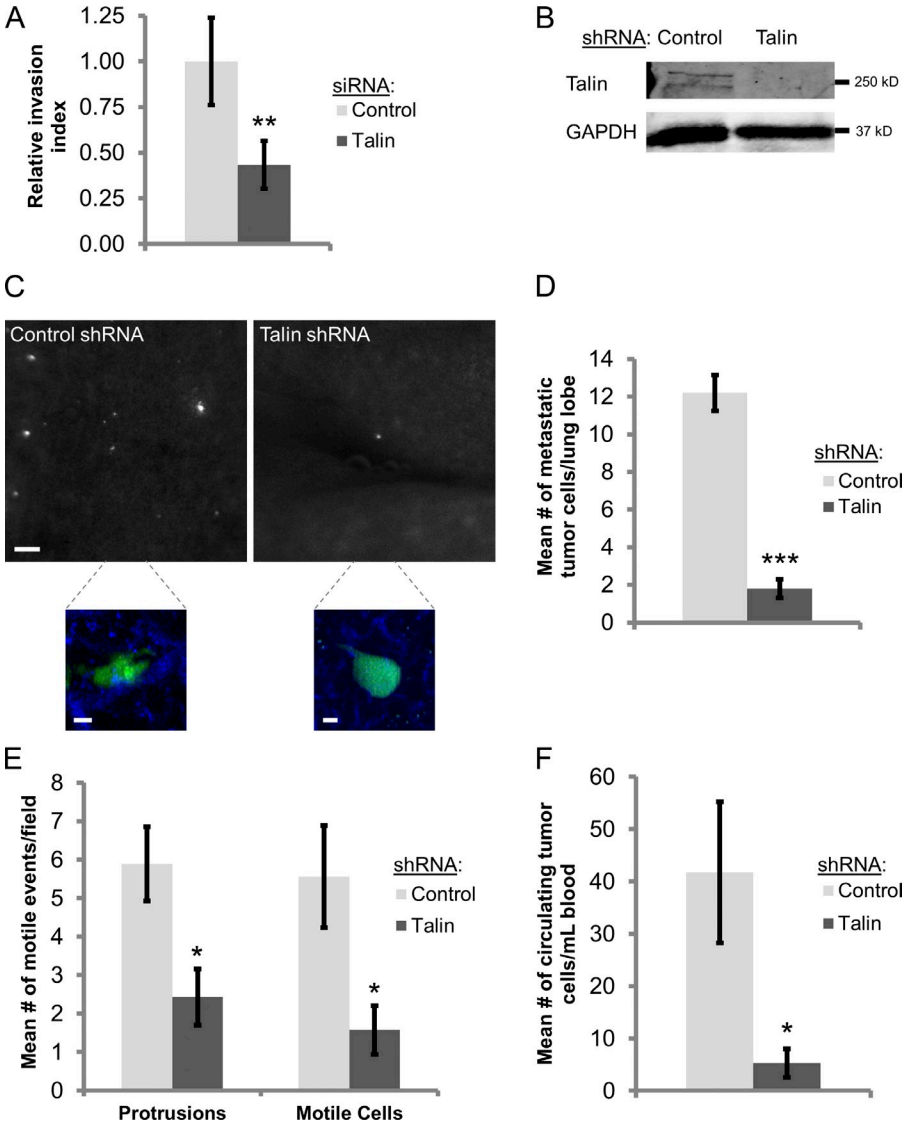

Figure 6. **Talin promotes mammary tumor cell invasion, intravasation, and lung metastasis.** (A) Inverted 3D ECM invasion assay. MDA-MB-231 cells were treated with control or talin siRNA and plated on the bottom of transwell filters and allowed to migrate into the 3D collagen/Matrigel matrix over the course of 4 d. The relative invasion index was quantified as the number of cells migrating above 60 µm/the number of cells below 30 µm. $n > 30$ cells; three independent experiments. **, $P < 0.029$. (B) Western blot analysis of MTLn3 cells stably expressing control or talin shRNA. Blots were stained for talin and GAPDH (loading control). (C and D) Spontaneous lung metastasis assay. (C) Representative fields of lungs from severe combined immunodeficiency mice harboring MTLn3-Dendra2 tumors expressing either control or talin shRNA. Bar, 200 µm. (bottom) Maximum intensity projection multiphoton image of control and talin shRNA metastatic MTLn3 tumor cells (green) that have extravasated into the lung parenchyma (second harmonic collagen; blue). Bars, 40 µm. (D) Quantification of the number of metastatic tumor cells per lung lobe in control or talin shRNA mice. $n = 5$ mice; ***, $P = 6.4 \times 10^{-5}$. (E) Quantification of the number of motile cells and protrusions per 100-µm field (see Videos 3 and 4). *, $P < 0.036$. (F) Quantification of the number of circulating tumor cells per millimeter of blood in control or talin shRNA mice. $n = 5$ mice; *, $P = 0.045$. Error bars represent the SEM.

maturation (i.e., actin polymerization and matrix degradation). Furthermore, talin is essential for tumor cell invasion through 3D ECM, intravasation, and spontaneous lung metastasis in vivo. As invadopodia degrade the ECM at sites of transendothelial migration in vitro and along blood vessels in vivo (Gligorijevic et al., 2012; Roh-Johnson et al., 2013), impaired invadopodium maturation likely accounts for the reductions in intravasation and metastasis in talin-depleted tumors in vivo, although we cannot exclude that talin also regulates in vivo focal adhesion formation (Zhang et al., 2008; Geraldo et al., 2012).

Recently, there is increasing evidence that focal adhesion proteins regulate tumor cell invasion by promoting invadopodium maturation (Branch et al., 2012; Pignatelli et al., 2012b; Beaty et al., 2013). β1 integrin and talin localize to the invadopodium core and are required to stabilize the structure (Beaty et al., 2013). Interestingly, talin binding to β1 integrin is not required for its initial recruitment, but this interaction is essential for invadopodium maturation. Given this data, we propose the following model of talin-dependent invadopodium maturation (Fig. 7): growth factors and other extracellular cues (e.g., hypoxia) induce invadopodium precursor formation (Lucien et al., 2011; Díaz et al., 2013), which occurs in a β1 integrin– and talin-independent manner (Fig. 7, stage 1). Talin is initially recruited to precursors by binding to actin via its C-terminal I/LWEQ actin binding domain, which is independent of binding to β1 integrin or moesin (Fig. 7, stage 2). Because the integrin binding site in the talin rod domain (integrin binding site 2) reinforces the linkage between integrins and the actin cytoskeleton and is thought to preferentially bind activated, high-affinity integrins (Moes et al., 2007; Rodius et al., 2008; Ellis et al., 2011), talin likely stabilizes invadopodia by binding to β1 integrin to anchor the invadopodium precursor structure to the ECM for initiation of the maturation process. Talin binding to β1 integrin also enhances the talin–moesin interaction, resulting in moesin enrichment at invadopodia (Fig. 7, stage 3). Moesin, in turn, recruits NHE-1 to invadopodia to disrupt the inhibitory, pH-dependent interaction between cortactin and cofilin and induce cofilin-Arp2/3–dependent actin polymerization (Fig. 7, stage 3; Oser et al., 2009; Magalhaes et al., 2011). Actin polymerization further stabilizes the invadopodium, and MT1-MMP and other

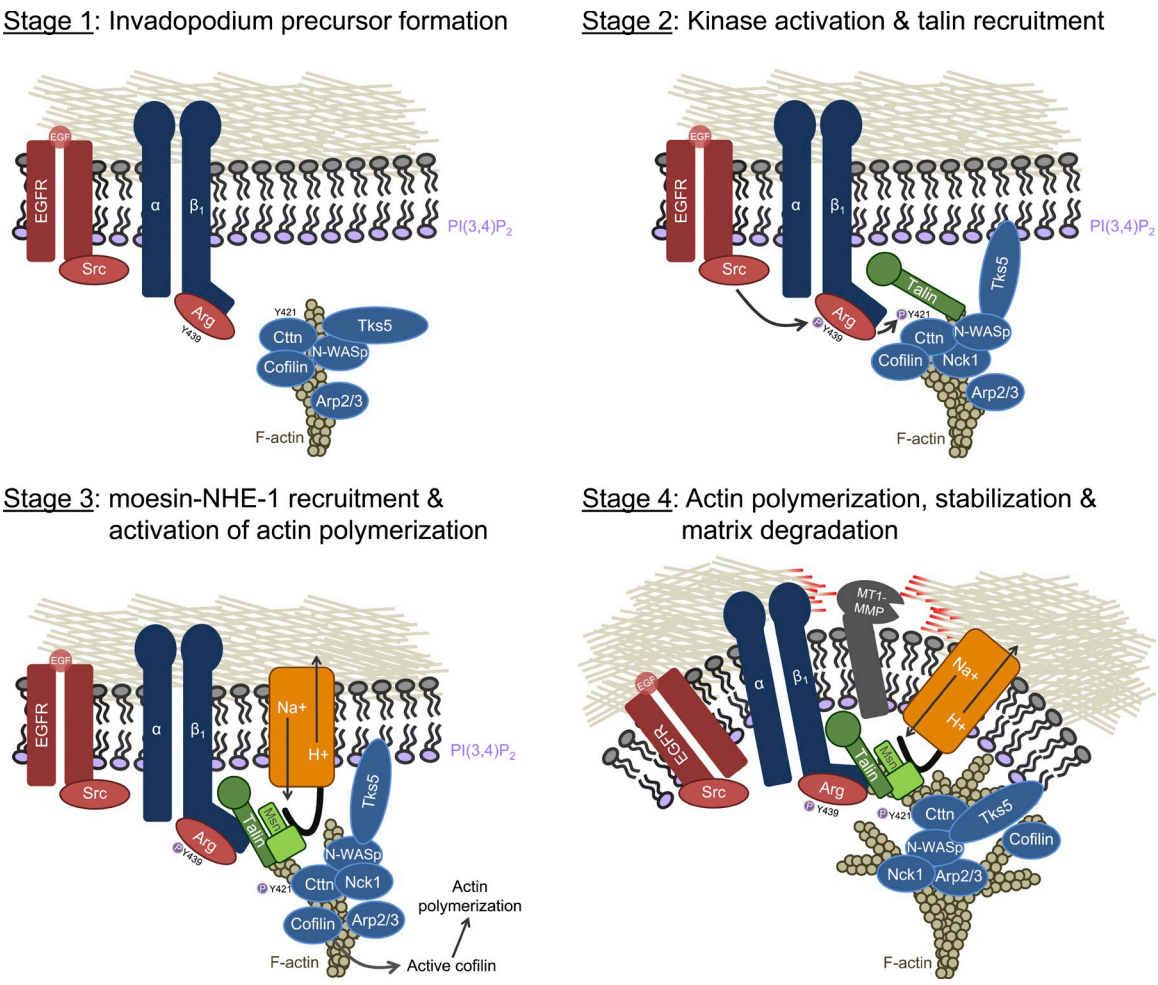

Figure 7. **Model of invadopodium maturation.** (stage 1) The invadopodium precursor assembles in response to growth factor stimulation (core structure consists of actin, cortactin [Cttn], cofilin, N-WASp, Arp2/3, and Tks5). During this time, kinases (Src and Arg) are also recruited. Between stage 1 and 2, Tks5 anchors the core structure to PI(3,4)P_2 at the invadopodium core (surrounding membrane not shown; Sharma et al., 2013a). (stage 2) After growth factor stimulation, Arg binding to β1 integrin disrupts the Arg autoinhibited conformation and growth factor receptors induce Src-dependent Arg phosphorylation on tyrosine 439 (Y439), resulting in full Arg kinase activation and phosphorylation of Y421 on cortactin (Beaty et al., 2013). Nck1 localizes to invadopodia by binding to phosphorylated cortactin and N-WASp (Oser et al., 2010). Talin is recruited to invadopodia in an integrin- and moesin (msn)-independent manner by binding to actin via its C-terminal I/LWEQ binding site. (stage 3) Talin binds to β1 integrin, which enhances the interaction between the talin rod domain (R11-DD) and the moesin FERM domain, to recruit a complex of moesin–NHE-1 to invadopodia. NHE-1 increases the intracellular pH to disrupt the inhibitory pH-dependent interaction between cortactin and cofilin, allowing active cofilin to be released. Cofilin severs F-actin to generate free actin barbed ends and new filament elongation. (stage 4) The new cofilin-generated filaments support dendritic nucleation by the Nck1–N-WASP–Arp2/3 complex. This actin polymerization, in turn, induces invadopodial membrane protrusion. MT1-MMP is locally delivered to invadopodia and activated to degrade the ECM either directly or indirectly through activation of pro-MMP-2 and -9 zymogens (Sakurai-Yageta et al., 2008).

proteases are recruited to degrade the ECM (Fig. 7, stage 4; Mueller et al., 1999; Yamaguchi et al., 2005; Artym et al., 2006; Clark et al., 2007; Sakurai-Yageta et al., 2008).

Talin and moesin are members of the FERM superfamily of proteins, which contain homologous FERM domains in the globular head domain, followed by elongated rod-like domains (Xing et al., 2001; Fehon et al., 2010; Shattil et al., 2010; Calderwood et al., 2013). Similar to the heterotypic interaction between the FERM family protein merlin and ezrin (Grönholm et al., 1999), in vitro binding assays indicate that talin and moesin bind in an antiparallel fashion, such that the talin C terminus (R11-DD) binds to the moesin FERM domain (N terminus). Interestingly, the moesin binding site on talin overlaps with both the integrin binding site 2 (R11-12) and F-actin binding sites (R13-DD; McLachlan et al., 1994; Hemmings et al., 1996; Gingras et al., 2009). Although it appears that the talin–β1 integrin interaction enhances talin–moesin binding (Fig. S4 A), future work will be required to determine if these binding interactions are competitive or cooperative.

Cellular modulation of intracellular and extracellular pH is central to tumor cell migration and invasion (Putney et al., 2002; Cardone et al., 2005; Webb et al., 2011; Amith and Fliegel, 2013). We provide evidence that talin is a novel upstream regulator of moesin–NHE-1 subcellular distribution and activity. Although the present study centers around talin-mediated regulation of NHE-1 at invadopodia, it will be interesting to explore whether this interaction is relevant at other structures including lamellipodial focal complexes and whether adhesion-based talin–NHE-1 complexes locally modulate intracellular pH in response to ECM stiffness and other extracellular cues to guide cell migration.

Materials and methods

Cell culture

MDA-MB-231 cells were obtained from American Type Culture Collection and cultured in DMEM/10% FBS. MTLn3 cells were cultured in αMEM/5% FBS. For EGF stimulation experiments, MDA-MB-231 cells were starved for 16 h in 0.5% FBS and 0.8% BSA in DMEM, and then for 10 min in L15 media/0.345% BSA. Cells were then stimulated with 2.5 nM EGF. MTLn3 were starved for 4 h in L15 media/0.345% BSA and then stimulated with 5 nM EGF.

Antibodies and reagents

The 8d4 talin-1/-2 antibody was purchased from Sigma-Aldrich (mouse). The Cortactin (goat), Tks5 (rabbit), Arp2 (rabbit), and GAPDH (rabbit) antibodies were obtained from Santa Cruz Biotechnology, Inc. The moesin antibodies were purchased from BD (mouse) and Cell Signaling Technology. The ezrin antibodies were obtained from Santa Cruz Biotechnology, Inc. (mouse) and Cell Signaling Technology (rabbit). The radixin and goat polyclonal internal talin antibodies were obtained from GeneTex (rabbit). The pan-phospho-threonine-ERM antibody was obtained from Cell Signaling Technology (rabbit). The chicken C-terminal (aa 639–815) NHE-1 antibody was a gift from D. Barber (University of California San Francisco, San Francisco, CA) and was used for Western blotting (Yan et al., 2001). The NHE-1 antibody used for immunofluorescence was obtained from Alpha Diagnostics (rabbit; NHE11-A). The TA205 talin head antibody was obtained from Enzo Life Sciences (mouse). The anti-His antibody was purchased from Thermo Fisher Scientific (mouse). The β1 integrin antibody (mouse) was purchased from BD. The FITC–anti-biotin antibody (mouse) was purchased from Jackson ImmunoResearch Laboratories, Inc. All Alexa Fluor secondary antibodies used were obtained from Molecular Probes. BCECF was obtained from Life Technologies.

DNA constructs, RNAi, and transfection

The GFP-talin constructs were obtained from Addgene (pEGFP-C1, CMV promoter; plasmids 26724, 32856, and 32855; A. Huttenlocher, University of Wisconsin, Madison, WI). The moesin-GFP constructs were also obtained from Addgene (pEGFP-N1, CMV promoter; plasmids 20677 and 20677; S. Shaw, National Cancer Institute, Besthesda, MD). The talin rod-GFP construct was subsequently mutated using site-directed mutagenesis (Quickchange I; Agilent Technologies), using the following primers: 5′-CCAAGGCCCTGGGTGACGCCGCCAGCGCTACGAAGGCTG-3′ and 5′-CAGCCTTCGTAGCGCTGGCGGCGTCACCCAGGGCCTTGG-3′ (L2094A/I2095A mutant) or 5′-CTCAGCTCCTGGTAGCTTGCGATGACGATGCAGATCAGGACTCTGAGGC-3′ and 5′-GCCTCAGAGTCCTGATCTGCATCGTCATCGCAAGCTACCAGGAGCTGAG-3′ (KVK/D mutant). The talin template (pJ6; rat β-actin promoter) used to generate the His-tagged talin fragments was provided by D. Calderwood (Yale University, New Haven, CT). The GST-tagged full-length moesin and N- and C-terminal fragments were purchased from Addgene (pGEX4T1, tac promoter; plasmids 11637, 11638, and 11639; V. Ramesh, Massachusetts General Hospital, Boston, MA). TagRFP-cortactin was described previously (N1-TagRFP, CMV promoter; Oser et al., 2009) and GFP-Tks5 was provided by S. Courtneidge (Burnham Institute for Medical Research, La Jolla, CA; pEGFP-C1, CMV promoter; Stylli et al., 2009). The Dendra2 construct has been described previously (pEGFP-C1, CMV promoter; Kedrin et al., 2008). Talin, moesin, ezrin, and β1 integrin siRNA were purchased from Thermo Fisher Scientific (siGENOME SMARTpool and siGENOME, respectively). All MDA-MB-231 transfections were performed by resuspending 10^6 in a 100-µl Lonza kit V transfection solution with either 2 µg DNA or 2 µM siRNA. Fluorescent proteins were allowed to express for 24 h before imaging. Cells were transfected with siRNA for 72 or 96 h.

Invadopodial matrix degradation assay, immunofluorescence, and fixation protocols

Gelatin (Sigma-Aldrich) was labeled with Alexa Fluor 405 (Invitrogen) according to the manufacturer's protocol (Sharma et al., 2013b). Mattek dishes were coated with a thin, 50-nm layer of gelatin as described previously (Mader et al., 2011; Magalhaes et al., 2011). In brief, dishes were treated with 50 µg/ml poly-L-lysine for 20 min and coated with 0.2% gelatin (in PBS) with 1:40 405-labeled gelatin for 10 min. Dishes were treated with 0.01% glutaraldehyde for 15 min and then treated with 5mg/ml sodium borohydride for 15 min. MDA-MB-231 cells were plated on 405-gelatin for 4 h (MTLn3 cells, 16 h) before fixation with 4% PFA. Cells were permeabilized with 0.1% Triton X-100 (or 0.5% Triton X-100 for talin staining) for 5 min, blocked with 1% FBS/1% BSA in PBS, and then stained with primary and secondary antibodies in blocking buffer, each for 1 h. Cells were then imaged in PBS at room temperature using the DeltaVision Core Microscope (Applied Precision; CoolSnap HQ2 camera, 60× NA, 1.4 oil objective, standard 4-channel filter set, and softWoRx software), laser scanning confocal microscope (LSM5 LIVE DuoScan; Carl Zeiss; 63× NA, 1.4 oil objective, AIM 4.2), or total internal reflection fluorescence microscope (TIRF; IX71; Olympus; Andor iXon Camera, 60× NA, 1.45 oil objective, MetaMorph; Gu et al., 2012).

Invadopodial lifetime assay

MDA-MB-231 cells were treated with control or talin siRNA for 72 h, transfected with TagRFP-cortactin and GFP-Tks5 for 24 h, and then plated on 405-labeled gelatin for 1.5 h before imaging. Cells were imaged in L15/10% FBS in a 37°C heated chamber using the DeltaVision Core Microscope (Applied Precision). GFP and RFP channels were acquired every 2 min, whereas 405-labeled gelatin was acquired every 10 min using a custom macro in the softWoRx software. Movies were acquired for 3 h. Cortactin-/Tks5-rich invadopodium lifetimes were quantified in ImageJ using Invadopodia Tracker plugin (Sharma et al., 2013b). Precursors were defined as cortactin-/Tks5-rich structures that did not colocalize with a matrix degradation hole, whereas mature invadopodia were defined as the structures that did colocalize with degradation holes.

Quantitative immunofluorescence

For quantitative immunofluorescence, cells from each sample were imaged using the same laser intensity and exposure time. Protein enrichment was quantified in ImageJ using background-subtracted images by measuring the mean fluorescent intensity (MFI) within the invadopodium core divided by the MFI in the surrounding cytosol: (protein of interest $MFI_{invadopodia\ -\ BG}$/protein of interest $MFI_{surrounding\ cytosol\ -\ BG}$) − 1 (Ellis et al., 2011; Beaty et al., 2013).

Intracellular pH measurements

Intracellular pH was measured as described previously (Frantz et al., 2008). In brief, the BCECF dye was resuspended in anhydrous DMSO (Life Technologies), and MDA-MB-231 cells were loaded with 5 µM BCECF in serum-free L15 media for 30 min. BCECF was imaged using a custom built TIRF microscope using 490- or 440-nm excitation and fixed emission at 535 nm. A ratio of the 490 nm/440 nm emission was used to calculate pH. BCECF emission ratios were calibrated by treating cells with a high K^+ media (105 mM KCl, 20 mM $CaCl_2$, 1 mM $MgSO_4$, 10 mM Hepes, 10 mM glucose, and TRIS for pH adjustment) with 10 µM nigericin at a series of different pH values (6.6, 6.8, 7, 7.2, and 7.4) and measuring the 490/440 nm emission (per the manufacturer's instructions). BCECF pH values obtained from imaging control and talin siRNA-treated cells were calibrated according to the manufacturer's instructions and as described previously (Frantz et al., 2008).

Coimmunoprecipitation and Western blotting

For coimmunoprecipitation experiments, MDA-MB-231 cells were starved and then stimulated with EGF for 3 min. Cells were washed with PBS and lysed using the following IP buffer: 20 mM Tris, pH 7.6, 100 mM NaCl, 1 mM EDTA, 10% glycerol, and 1% NP-40 with protease and phosphatase inhibitor cocktails, modified from Pignatelli et al. (2012a). Lysates were centrifuged at 14,000 rpm for 10 min at 4°C and then cleared with protein A/G beads (Santa Cruz, Biotechnology, Inc.) for 20 min. Lysates were then incubated with the 8d4 talin antibody for 9 h before the beads were added for 9 h. The beads were washed, and the samples were run on an SDS-PAGE gel. Blots were probed for NHE-1, moesin, or ezrin. Protein was then transferred to nitrocellulose paper, blocked using Odyssey solution (LI-COR Biosciences) and immunostained. All primary and secondary antibodies were diluted in Odyssey blocking solution and detected using the Odyssey scanner.

Direct binding assay

GST-moesin constructs were fused to glutathione-Sepharose beads as described previously (Bravo-Cordero et al., 2013). In brief, GST-moesin (pGEX4T1, tac promoter) was expressed in *Escherichia coli* and purified using glutathione-agarose beads. Talin fragments constituting the talin head domain (aa 1–433), talin rod R1–5 (aa 434–1,203), talin rod R6–10 (aa 1,205–1,971), or talin rod R11-DD (aa 1,975–2,541), R11 (aa 1,975–2,140), R12 (aa 2,141–2,291), and R13-DD (aa 2,300–2,541) were generated by PCR, excised with BamHI or SalI and NotI, and cloned into the pET30a vector (EMD Millipore). The resulting constructs were expressed in *E. coli* BL21, and protein expression was induced with 0.2 mM IPTG as described previously (Xing et al., 2001). Recombinant his-tagged talin protein was then purified using a HisTALON column according to the manufacturer's instructions (Takara Bio Inc.). Protein concentration was

determined and 1 µg of recombinant talin was added to 50 µl of GST-moesin beads for 2 h at 4°C, washed to remove unbound protein, and run on SDS-PAGE, as described previously (Lad et al., 2007; Gingras et al., 2009; Bouaouina et al., 2012).

Barbed end assay

The barbed end assay was performed as described previously (Chan et al., 1998; Oser et al., 2010; Mader et al., 2011). In brief, cells were starved and then stimulated with EGF as described in the Cell culture section. Cells were then permeabilized with 20 mM Hepes, pH 7.5, 138 mM KCl, 4 mM $MgCl_2$, 3 mM EGTA, 0.2 mg/ml saponin, 1 mM ATP, and 1% BSA, containing 0.4 µM biotinylated actin (Cytoskeleton) for 1 min. Cells were fixed with 4% PFA in fix buffer for 5 min, treated with glycine for 10 min, and blocked for 20 min with 1% FBS/1% BSA/3 µM phalloidin in PBS before immunostaining with FITC–anti-biotin as well as cortactin and Arp2 to identify invadopodium precursors. Cells were imaged on the DeltaVision Core Microscope, and the barbed end intensity at each invadopodium was determined by measuring FITC-biotin MFI in background-subtracted images.

Inverted 3D invasion assay

An inverted invasion assay was adapted from an established protocol (Hennigan et al., 1994; Caswell et al., 2007; Tuomi et al., 2009; Deakin and Turner, 2011). A 3D ECM containing 4.6 mg/ml of type I collagen (BD) and 2.2mg/ml Matrigel (Invitrogen) was pipetted onto the top surface of an 8-µm transwell filter. The matrix was allowed to polymerize for 1 h at 37°C. 50,000 MDA-MB-231 cells were plated on the bottom surface of the filter and allowed to attach for 30 min. The transwell was then placed in a 24-well dish with serum-free DMEM in the lower chamber and DMEM/10% FBS in the upper chamber. Cells invaded up into the 3D ECM for 4 d before fixation with 4% PFA and staining with Alexa Fluor 546–phalloidin (Life Technologies). Cells were imaged every 10 µm for 100 µm beginning at the filter using the laser scanning confocal microscope (LSM5 LIVE DuoScan). The relative invasion index was quantified as the number of cells migrating above 60 µm/the number of cells below 30 µm.

Animal model, circulating tumor cell, and spontaneous metastasis assays

All procedures were conducted in accordance with the National Institutes of Health regulations and approved by the Albert Einstein College of Medicine animal care and use committees. The stable MTLn3 control shRNA (targeting the sequence of GFP) and talin shRNA cell lines were generated using TRC shRNA lentiviral vectors (Thermo Fisher Scientific). Cells were then transfected with Dendra2 using Lipofectamine 2000 and selected using geneticin. After FACS sorting, cells were resuspended in PBS at a concentration of 10^6 and injected into the mammary fat pad of severe combined immunodeficiency mice (Roussos et al., 2011). After 4 wk, animals were anesthetized, 1 ml of blood was extracted by cardiac puncture, and the primary tumor and lung were excised (Wyckoff et al., 2000). Surface lung metastases were quantified by counting the number of single, Dendra2+ MTLn3 cells per lung lobe using the stereo microscope (Olympus) at low magnification (Roussos et al., 2011). The lungs were then imaged at higher magnification on a custom-built multiphoton microscope to further confirm the identity of the cells (Entenberg et al., 2011). Primary tumor sizes were determined by measuring the width and length of the tumor with calipers and calculating the tumor size by the following formula: $V = 4/3\pi \times (\text{width}/2)^2 \times (\text{length}/2)$, which represents the 3D volume of an ellipse (Shimizu et al., 2010).

Time-lapse intravital imaging of tumor cell motility was conducted 3.5 wk after injection using the custom multiphoton microscope (Entenberg et al., 2011). Immediately before imaging, animals were injected with 100 µl of 150-kD rhodamine dextran into the tail vein (Fein and Egeblad, 2013; Kilarski et al., 2013). Images of tumor cells (Dendra2), collagen (second harmonic), and blood vessels (dextran) were acquired every 3 min for 1.5 h. Z-stacks were collected with a step size of 5 µm for 100 µm.

To quantify the number of circulating tumor cells, the blood burden assay was used (Wyckoff et al., 2000; Roussos et al., 2011). In brief, the blood extracted from the cardiac puncture was placed in αMEM/5% FBS for 24 h. The excess red blood cells were washed off and cells were grown in αMEM for six more days before counting.

Statistical analysis

Unpaired, two-tailed Student's *t* tests were used to determine significance. $P < 0.05$ was considered significant for all experiments. Error bars represent the SEM. Graphs are presented as mean ± SEM.

Online supplemental material

Fig. S1 shows when talin localizes to invadopodium precursors and demonstrates that the GFP-talin constructs are expressed to a similar level in MDA-MB-231 cells throughout the paper. Fig. S2 shows the effect of talin knockdown on cell spreading and focal adhesion formation. Fig. S3 shows that talin is required for barbed end formation and invadopodial matrix degradation in MTLn3 cells, similar to MDA-MB-231 cells (see Figs. 1 and 5). Fig. S4 shows that β1 integrin does not affect talin localization to invadopodia, but is required for moesin and NHE-1 enrichment (via the talin–moesin interaction; Figs. 3 and 4). Fig. S4 also shows that phosphorylated ERM proteins localize to invadopodia, but ezrin and radixin do not and that ezrin and β1 integrin siRNA efficiently knocks down the proteins in MDA-MB-231 cells (see Fig. 4). Fig. S5 shows that moesin is not required for talin recruitment to invadopodia, talin is upstream of moesin in the NHE-1 invadopodium pathway, talin–moesin direct binding results, and the effect of talin knockdown on tumor growth in MTLn3 tumors in vivo (see Figs. 4 and 6). Videos 1 and 2 correspond to the lifetime analyses performed in Fig. 1 G. Videos 3 and 4 correspond to the in vivo tumor cell motility and protrusion analyses performed in Fig. 6 E. Online supplemental material is available at http://www.jcb.org/cgi/content/full/jcb.201312046/DC1.

We thank David Calderwood, Sara Courtneidge, and Diane Barber for providing us the talin DNA, GFP-Tks5 construct, and NHE-1 antibody, respectively. We also thank the Albert Einstein shRNA core facility for their guidance in generating the stable talin shRNA cell line and the Albert Einstein Genomics Core for their assistance with DNA sequencing. We are grateful to Jeanine Pignatelli for her assistance with the 3D ECM invasion assay. We thank Anthony Koleske and the Cox, Segall, and Hodgson laboratories for their thoughtful discussion. We also thank the Analytical Imaging Facility in the Gruss Lipper Biophotonics Center, especially Vera DesMarais and Peng Guo, for technical support.

This work was funded by National Institutes of Health (NIH) CA150344 (J. Condeelis), Medical Scientist Training Program grant T32-GM007288, Komen postdoctoral fellowship KG111405 (V.P. Sharma), NIH GM093121 (L. Hodgson), and NIH T32GM007491 (V. Miskolci).

The authors declare no competing financial interests.

Submitted: 12 December 2013
Accepted: 28 April 2014

References

Amith, S.R., and L. Fliegel. 2013. Regulation of the Na^+/H^+ exchanger (NHE1) in breast cancer metastasis. *Cancer Res.* 73:1259–1264. http://dx.doi.org/10.1158/0008-5472.CAN-12-4031

Antelmi, E., R.A. Cardone, M.R. Greco, R. Rubino, F. Di Sole, N.A. Martino, V. Casavola, M. Carcangiu, L. Moro, and S.J. Reshkin. 2013. ß1 integrin binding phosphorylates ezrin at T567 to activate a lipid raft signalsome driving invadopodia activity and invasion. *PLoS ONE.* 8:e75113. http://dx.doi.org/10.1371/journal.pone.0075113

Anthis, N.J., K.L. Wegener, F. Ye, C. Kim, B.T. Goult, E.D. Lowe, I. Vakonakis, N. Bate, D.R. Critchley, M.H. Ginsberg, and I.D. Campbell. 2009. The structure of an integrin/talin complex reveals the basis of inside-out signal transduction. *EMBO J.* 28:3623–3632. http://dx.doi.org/10.1038/emboj.2009.287

Artym, V.V., Y. Zhang, F. Seillier-Moiseiwitsch, K.M. Yamada, and S.C. Mueller. 2006. Dynamic interactions of cortactin and membrane type 1 matrix metalloproteinase at invadopodia: defining the stages of invadopodia formation and function. *Cancer Res.* 66:3034–3043. http://dx.doi.org/10.1158/0008-5472.CAN-05-2177

Bakolitsa, C., D.M. Cohen, L.A. Bankston, A.A. Bobkov, G.W. Cadwell, L. Jennings, D.R. Critchley, S.W. Craig, and R.C. Liddington. 2004. Structural basis for vinculin activation at sites of cell adhesion. *Nature.* 430:583–586. http://dx.doi.org/10.1038/nature02610

Beaty, B.T., V.P. Sharma, J.J. Bravo-Cordero, M.A. Simpson, R.J. Eddy, A.J. Koleske, and J. Condeelis. 2013. β1 integrin regulates Arg to promote invadopodial maturation and matrix degradation. *Mol. Biol. Cell.* 24:1661–1675: S1–S11. http://dx.doi.org/10.1091/mbc.E12-12-0908

Bouaouina, M., B.T. Goult, C. Huet-Calderwood, N. Bate, N.N. Brahme, I.L. Barsukov, D.R. Critchley, and D.A. Calderwood. 2012. A conserved lipid-binding loop in the kindlin FERM F1 domain is required for kindlin-mediated αIIbβ3 integrin coactivation. *J. Biol. Chem.* 287:6979–6990. http://dx.doi.org/10.1074/jbc.M111.330845

Branch, K.M., D. Hoshino, and A.M. Weaver. 2012. Adhesion rings surround invadopodia and promote maturation. *Biol. Open.* 1:711–722. http://dx.doi.org/10.1242/bio.20121867

Bravo-Cordero, J.J., L. Hodgson, and J. Condeelis. 2012. Directed cell invasion and migration during metastasis. *Curr. Opin. Cell Biol.* 24:277–283. http://dx.doi.org/10.1016/j.ceb.2011.12.004

Bravo-Cordero, J.J., V.P. Sharma, M. Roh-Johnson, X. Chen, R. Eddy, J. Condeelis, and L. Hodgson. 2013. Spatial regulation of RhoC activity defines protrusion formation in migrating cells. *J. Cell Sci.* 126:3356–3369. http://dx.doi.org/10.1242/jcs.123547

Brisson, L., V. Driffort, L. Benoist, M. Poet, L. Counillon, E. Antelmi, R. Rubino, P. Besson, F. Labbal, S. Chevalier, et al. 2013. $Na_V1.5$ Na^+ channels allosterically regulate the NHE-1 exchanger and promote the activity of breast cancer cell invadopodia. *J. Cell Sci.* 126:4835–4842. http://dx.doi.org/10.1242/jcs.123901

Burridge, K., and L. Connell. 1983. A new protein of adhesion plaques and ruffling membranes. *J. Cell Biol.* 97:359–367. http://dx.doi.org/10.1083/jcb.97.2.359

Burridge, K., and P. Mangeat. 1984. An interaction between vinculin and talin. *Nature*. 308:744–746. http://dx.doi.org/10.1038/308744a0

Busco, G., R.A. Cardone, M.R. Greco, A. Bellizzi, M. Colella, E. Antelmi, M.T. Mancini, M.E. Dell'Aquila, V. Casavola, A. Paradiso, and S.J. Reshkin. 2010. NHE1 promotes invadopodial ECM proteolysis through acidification of the peri-invadopodial space. *FASEB J.* 24:3903–3915. http://dx.doi.org/10.1096/fj.09-149518

Calderwood, D.A., R. Zent, R. Grant, D.J.G. Rees, R.O. Hynes, and M.H. Ginsberg. 1999. The Talin head domain binds to integrin β subunit cytoplasmic tails and regulates integrin activation. *J. Biol. Chem.* 274:28071–28074. http://dx.doi.org/10.1074/jbc.274.40.28071

Calderwood, D.A., I.D. Campbell, and D.R. Critchley. 2013. Talins and kindlins: partners in integrin-mediated adhesion. *Nat. Rev. Mol. Cell Biol.* 14:503–517. http://dx.doi.org/10.1038/nrm3624

Cameron, M.D., E.E. Schmidt, N. Kerkvliet, K.V. Nadkarni, V.L. Morris, A.C. Groom, A.F. Chambers, and I.C. MacDonald. 2000. Temporal progression of metastasis in lung: cell survival, dormancy, and location dependence of metastatic inefficiency. *Cancer Res.* 60:2541–2546.

Cardone, R.A., V. Casavola, and S.J. Reshkin. 2005. The role of disturbed pH dynamics and the Na^+/H^+ exchanger in metastasis. *Nat. Rev. Cancer*. 5:786–795. http://dx.doi.org/10.1038/nrc1713

Caswell, P.T., H.J. Spence, M. Parsons, D.P. White, K. Clark, K.W. Cheng, G.B. Mills, M.J. Humphries, A.J. Messent, K.I. Anderson, et al. 2007. Rab25 associates with α5β1 integrin to promote invasive migration in 3D microenvironments. *Dev. Cell*. 13:496–510. http://dx.doi.org/10.1016/j.devcel.2007.08.012

Chan, A.Y., S. Raft, M. Bailly, J.B. Wyckoff, J.E. Segall, and J.S. Condeelis. 1998. EGF stimulates an increase in actin nucleation and filament number at the leading edge of the lamellipod in mammary adenocarcinoma cells. *J. Cell Sci.* 111:199–211.

Chan, K.T., C.L. Cortesio, and A. Huttenlocher. 2009. FAK alters invadopodia and focal adhesion composition and dynamics to regulate breast cancer invasion. *J. Cell Biol.* 185:357–370. http://dx.doi.org/10.1083/jcb.200809110

Choi, C.-H., B.A. Webb, M.S. Chimenti, M.P. Jacobson, and D.L. Barber. 2013. pH sensing by FAK-His58 regulates focal adhesion remodeling. *J. Cell Biol.* 202:849–859. http://dx.doi.org/10.1083/jcb.201302131

Clark, E.S., A.S. Whigham, W.G. Yarbrough, and A.M. Weaver. 2007. Cortactin is an essential regulator of matrix metalloproteinase secretion and extracellular matrix degradation in invadopodia. *Cancer Res.* 67:4227–4235. http://dx.doi.org/10.1158/0008-5472.CAN-06-3928

Deakin, N.O., and C.E. Turner. 2011. Distinct roles for paxillin and Hic-5 in regulating breast cancer cell morphology, invasion, and metastasis. *Mol. Biol. Cell*. 22:327–341. http://dx.doi.org/10.1091/mbc.E10-09-0790

Denker, S.P., D.C. Huang, J. Orlowski, H. Furthmayr, and D.L. Barber. 2000. Direct binding of the Na—H exchanger NHE1 to ERM proteins regulates the cortical cytoskeleton and cell shape independently of H^+ translocation. *Mol. Cell*. 6:1425–1436. http://dx.doi.org/10.1016/S1097-2765(00)00139-8

DesMarais, V., F. Macaluso, J. Condeelis, and M. Bailly. 2004. Synergistic interaction between the Arp2/3 complex and cofilin drives stimulated lamellipod extension. *J. Cell Sci.* 117:3499–3510. http://dx.doi.org/10.1242/jcs.01211

Dhruv, H.D., W.S. McDonough Winslow, B. Armstrong, S. Tuncali, J. Eschbacher, K. Kislin, J.C. Loftus, N.L. Tran, and M.E. Berens. 2013. Reciprocal activation of transcription factors underlies the dichotomy between proliferation and invasion of glioma cells. *PLoS ONE*. 8:e72134. http://dx.doi.org/10.1371/journal.pone.0072134

Díaz, B., A. Yuen, S. Iizuka, S. Higashiyama, and S.A. Courtneidge. 2013. Notch increases the shedding of HB-EGF by ADAM12 to potentiate invadopodia formation in hypoxia. *J. Cell Biol.* 201:279–292. http://dx.doi.org/10.1083/jcb.201209151

Eckert, M.A., T.M. Lwin, A.T. Chang, J. Kim, E. Danis, L. Ohno-Machado, and J. Yang. 2011. Twist1-induced invadopodia formation promotes tumor metastasis. *Cancer Cell*. 19:372–386. http://dx.doi.org/10.1016/j.ccr.2011.01.036

Elliott, P.R., B.T. Goult, P.M. Kopp, N. Bate, J.G. Grossmann, G.C.K. Roberts, D.R. Critchley, and I.L. Barsukov. 2010. The Structure of the talin head reveals a novel extended conformation of the FERM domain. *Structure*. 18:1289–1299. http://dx.doi.org/10.1016/j.str.2010.07.011

Ellis, S.J., M. Pines, M.J. Fairchild, and G. Tanentzapf. 2011. In vivo functional analysis reveals specific roles for the integrin-binding sites of talin. *J. Cell Sci.* 124:1844–1856. http://dx.doi.org/10.1242/jcs.083337

Entenberg, D., J. Wyckoff, B. Gligorijevic, E.T. Roussos, V.V. Verkhusha, J.W. Pollard, and J. Condeelis. 2011. Setup and use of a two-laser multiphoton microscope for multichannel intravital fluorescence imaging. *Nat. Protoc.* 6:1500–1520. http://dx.doi.org/10.1038/nprot.2011.376

Estecha, A., L. Sánchez-Martín, A. Puig-Kröger, R.A. Bartolomé, J. Teixidó, R. Samaniego, and P. Sánchez-Mateos. 2009. Moesin orchestrates cortical polarity of melanoma tumour cells to initiate 3D invasion. *J. Cell Sci.* 122:3492–3501. http://dx.doi.org/10.1242/jcs.053157

Fehon, R.G., A.I. McClatchey, and A. Bretscher. 2010. Organizing the cell cortex: the role of ERM proteins. *Nat. Rev. Mol. Cell Biol.* 11:276–287. http://dx.doi.org/10.1038/nrm2866

Fein, M.R., and M. Egeblad. 2013. Caught in the act: revealing the metastatic process by live imaging. *Dis. Model. Mech.* 6:580–593. http://dx.doi.org/10.1242/dmm.009282

Franco, S.J., M.A. Rodgers, B.J. Perrin, J.W. Han, D.A. Bennin, D.R. Critchley, and A. Huttenlocher. 2004. Calpain-mediated proteolysis of talin regulates adhesion dynamics. *Nat. Cell Biol.* 6:977–983. http://dx.doi.org/10.1038/ncb1175

Franco, S.J., M.A. Senetar, W.T.N. Simonson, A. Huttenlocher, and R.O. McCann. 2006. The conserved C-terminal I/LWEQ module targets Talin1 to focal adhesions. *Cell Motil. Cytoskeleton*. 63:563–581. http://dx.doi.org/10.1002/cm.20145

Frantz, C., G. Barreiro, L. Dominguez, X.M. Chen, R. Eddy, J. Condeelis, M.J.S. Kelly, M.P. Jacobson, and D.L. Barber. 2008. Cofilin is a pH sensor for actin free barbed end formation: role of phosphoinositide binding. *J. Cell Biol.* 183:865–879. http://dx.doi.org/10.1083/jcb.200804161

Gaggioli, C., S. Hooper, C. Hidalgo-Carcedo, R. Grosse, J.F. Marshall, K. Harrington, and E. Sahai. 2007. Fibroblast-led collective invasion of carcinoma cells with differing roles for RhoGTPases in leading and following cells. *Nat. Cell Biol.* 9:1392–1400. http://dx.doi.org/10.1038/ncb1658

Geraldo, S., A. Simon, N. Elkhatib, D. Louvard, L. Fetler, and D.M. Vignjevic. 2012. Do cancer cells have distinct adhesions in 3D collagen matrices and in vivo? *Eur. J. Cell Biol.* 91:930–937. http://dx.doi.org/10.1016/j.ejcb.2012.07.005

Gil-Henn, H., A. Patsialou, Y. Wang, M.S. Warren, J.S. Condeelis, and A.J. Koleske. 2013. Arg/Abl2 promotes invasion and attenuates proliferation of breast cancer in vivo. *Oncogene*. 32:2622–2630. http://dx.doi.org/10.1038/onc.2012.284

Gingras, A.R., N. Bate, B.T. Goult, L. Hazelwood, I. Canestrelli, J.G. Grossmann, H. Liu, N.S.M. Putz, G.C.K. Roberts, N. Volkmann, et al. 2008. The structure of the C-terminal actin-binding domain of talin. *EMBO J.* 27:458–469. http://dx.doi.org/10.1038/sj.emboj.7601965

Gingras, A.R., W.H. Ziegler, A.A. Bobkov, M.G. Joyce, D. Fasci, M. Himmel, S. Rothemund, A. Ritter, J.G. Grossmann, B. Patel, et al. 2009. Structural determinants of integrin binding to the talin rod. *J. Biol. Chem.* 284:8866–8876. http://dx.doi.org/10.1074/jbc.M805937200

Gingras, A.R., N. Bate, B.T. Goult, B. Patel, P.M. Kopp, J. Emsley, I.L. Barsukov, G.C.K. Roberts, and D.R. Critchley. 2010. Central region of talin has a unique fold that binds vinculin and actin. *J. Biol. Chem.* 285:29577–29587. http://dx.doi.org/10.1074/jbc.M109.095455

Gligorijevic, B., J. Wyckoff, H. Yamaguchi, Y. Wang, E.T. Roussos, and J. Condeelis. 2012. N-WASP-mediated invadopodium formation is involved in intravasation and lung metastasis of mammary tumors. *J. Cell Sci.* 125:724–734. http://dx.doi.org/10.1242/jcs.092726

Goksoy, E., Y.Q. Ma, X.X. Wang, X.M. Kong, D. Perera, E.F. Plow, and J. Qin. 2008. Structural basis for the autoinhibition of talin in regulating integrin activation. *Mol. Cell*. 31:124–133. http://dx.doi.org/10.1016/j.molcel.2008.06.011

Goldberg, S.F., J.F. Harms, K. Quon, and D.R. Welch. 1999. Metastasis-suppressed C8161 melanoma cells arrest in lung but fail to proliferate. *Clin. Exp. Metastasis*. 17:601–607. http://dx.doi.org/10.1023/A:1006718800891

Gonzalez-Agosti, C., T. Wiederhold, M.E. Herndon, J. Gusella, and V. Ramesh. 1999. Interdomain interaction of merlin isoforms and its influence on intermolecular binding to NHE-RF. *J. Biol. Chem.* 274:34438–34442. http://dx.doi.org/10.1074/jbc.274.48.34438

Goult, B.T., T. Zacharchenko, N. Bate, R. Tsang, F. Hey, A.R. Gingras, P.R. Elliott, G.C. Roberts, C. Ballestrem, D.R. Critchley, and I.L. Barsukov. 2013. RIAM and vinculin binding to talin are mutually exclusive and regulate adhesion assembly and turnover. *J. Biol. Chem.* 288:8238–8249. http://dx.doi.org/10.1074/jbc.M112.438119

Grönholm, M., M. Sainio, F. Zhao, L. Heiska, A. Vaheri, and O. Carpén. 1999. Homotypic and heterotypic interaction of the neurofibromatosis 2 tumor suppressor protein merlin and the ERM protein ezrin. *J. Cell Sci.* 112:895–904.

Gu, W., Z. Katz, B. Wu, H.Y. Park, D.L. Li, S. Lin, A.L. Wells, and R.H. Singer. 2012. Regulation of local expression of cell adhesion and motility-related mRNAs in breast cancer cells by IMP1/ZBP1. *J. Cell Sci.* 125:81–91. http://dx.doi.org/10.1242/jcs.086132

Helzer, K.T., H.E. Barnes, L. Day, J. Harvey, P.R. Billings, and A. Forsyth. 2009. Circulating tumor cells are transcriptionally similar to the primary tumor in a murine prostate model. *Cancer Res.* 69:7860–7866. http://dx.doi.org/10.1158/0008-5472.CAN-09-0801

Hemmings, L., D.J.G. Rees, V. Ohanian, S.J. Bolton, A.P. Gilmore, B. Patel, H. Priddle, J.E. Trevithick, R.O. Hynes, and D.R. Critchley. 1996. Talin contains three actin-binding sites each of which is adjacent to a vinculin-binding site. *J. Cell Sci.* 109:2715–2726.

Hennigan, R.F., K.L. Hawker, and B.W. Ozanne. 1994. Fos-transformation activates genes associated with invasion. *Oncogene*. 9:3591–3600.

Horwitz, A., K. Duggan, C. Buck, M.C. Beckerle, and K. Burridge. 1986. Interaction of plasma membrane fibronectin receptor with talin—a transmembrane linkage. *Nature*. 320:531–533. http://dx.doi.org/10.1038/320531a0

Huang, C., Z. Rajfur, N. Yousefi, Z.Z. Chen, K. Jacobson, and M.H. Ginsberg. 2009. Talin phosphorylation by Cdk5 regulates Smurf1-mediated talin head ubiquitylation and cell migration. *Nat. Cell Biol.* 11:624–630. http://dx.doi.org/10.1038/ncb1868

Huttenlocher, A., and A.R. Horwitz. 2011. Integrins in cell migration. *Cold Spring Harb. Perspect. Biol.* 3:a005074. http://dx.doi.org/10.1101/cshperspect.a005074

Jiang, G.Y., G. Giannone, D.R. Critchley, E. Fukumoto, and M.P. Sheetz. 2003. Two-piconewton slip bond between fibronectin and the cytoskeleton depends on talin. *Nature*. 424:334–337. http://dx.doi.org/10.1038/nature01805

Kedrin, D., B. Gligorijevic, J. Wyckoff, V.V. Verkhusha, J. Condeelis, J.E. Segall, and J. van Rheenen. 2008. Intravital imaging of metastatic behavior through a mammary imaging window. *Nat. Methods*. 5:1019–1021. http://dx.doi.org/10.1038/nmeth.1269

Kilarski, W.W., E. Güç, J.C.M. Teo, S.R. Oliver, A.W. Lund, and M.A. Swartz. 2013. Intravital immunofluorescence for visualizing the microcirculatory and immune microenvironments in the mouse ear dermis. *PLoS ONE*. 8:e57135. http://dx.doi.org/10.1371/journal.pone.0057135

Kim, C.H., F. Ye, X.H. Hu, and M.H. Ginsberg. 2012. Talin activates integrins by altering the topology of the β transmembrane domain. *J. Cell Biol.* 197:605–611. http://dx.doi.org/10.1083/jcb.201112141

Lad, Y., D.S. Harburger, and D.A. Calderwood. 2007. Integrin cytoskeletal interactions. *Methods Enzymol.* 426:69–84. http://dx.doi.org/10.1016/S0076-6879(07)26004-5

Li, A., J.C. Dawson, M. Forero-Vargas, H.J. Spence, X.Z. Yu, I. König, K. Anderson, and L.M. Machesky. 2010. The actin-bundling protein fascin stabilizes actin in invadopodia and potentiates protrusive invasion. *Curr. Biol.* 20:339–345. http://dx.doi.org/10.1016/j.cub.2009.12.035

Linder, S., C. Wiesner, and M. Himmel. 2011. Degrading devices: invadosomes in proteolytic cell invasion. *Annu. Rev. Cell Dev. Biol.* 27:185–211. http://dx.doi.org/10.1146/annurev-cellbio-092910-154216

Lucien, F., K. Brochu-Gaudreau, D. Arsenault, K. Harper, and C.M. Dubois. 2011. Hypoxia-induced invadopodia formation involves activation of NHE-1 by the p90 ribosomal S6 kinase (p90RSK). *PLoS ONE*. 6:e28851. http://dx.doi.org/10.1371/journal.pone.0028851

Mader, C.C., M. Oser, M.A.O. Magalhaes, J.J. Bravo-Cordero, J. Condeelis, A.J. Koleske, and H. Gil-Henn. 2011. An EGFR–Src–Arg–cortactin pathway mediates functional maturation of invadopodia and breast cancer cell invasion. *Cancer Res.* 71:1730–1741. http://dx.doi.org/10.1158/0008-5472.CAN-10-1432

Madsen, C.D., and E. Sahai. 2010. Cancer dissemination—lessons from leukocytes. *Dev. Cell*. 19:13–26. http://dx.doi.org/10.1016/j.devcel.2010.06.013

Magalhaes, M.A.O., D.R. Larson, C.C. Mader, J.J. Bravo-Cordero, H. Gil-Henn, M. Oser, X. Chen, A.J. Koleske, and J. Condeelis. 2011. Cortactin phosphorylation regulates cell invasion through a pH-dependent pathway. *J. Cell Biol.* 195:903–920. http://dx.doi.org/10.1083/jcb.201103045

McLachlan, A.D., M. Stewart, R.O. Hynes, and D.J.G. Rees. 1994. Analysis of repeated motifs in the talin rod. *J. Mol. Biol.* 235:1278–1290. http://dx.doi.org/10.1006/jmbi.1994.1081

Moes, M., S. Rodius, S.J. Coleman, S.J. Monkley, E. Goormaghtigh, L. Tremuth, C. Kox, P.P.G. van der Holst, D.R. Critchley, and N. Kieffer. 2007. The integrin binding site 2 (IBS2) in the talin rod domain is essential for linking integrin β subunits to the cytoskeleton. *J. Biol. Chem.* 282:17280–17288. http://dx.doi.org/10.1074/jbc.M611846200

Molony, L., D. McCaslin, J. Abernethy, B. Paschal, and K. Burridge. 1987. Properties of talin from chicken gizzard smooth muscle. *J. Biol. Chem.* 262:7790–7795.

Mueller, S.C., Y.Y. Yeh, and W.T. Chen. 1992. Tyrosine phosphorylation of membrane proteins mediates cellular invasion by transformed cells. *J. Cell Biol.* 119:1309–1325. http://dx.doi.org/10.1083/jcb.119.5.1309

Mueller, S.C., G. Ghersi, S.K. Akiyama, Q.X.A. Sang, L. Howard, M. Pineiro-Sanchez, H. Nakahara, Y. Yeh, and W.T. Chen. 1999. A novel protease-docking function of integrin at invadopodia. *J. Biol. Chem.* 274:24947–24952. http://dx.doi.org/10.1074/jbc.274.35.24947

Nakahara, H., S.C. Mueller, M. Nomizu, Y. Yamada, Y.Y. Yeh, and W.T. Chen. 1998. Activation of β1 integrin signaling stimulates tyrosine phosphorylation of $p190^{RhoGAP}$ and membrane-protrusive activities at invadopodia. *J. Biol. Chem.* 273:9–12. http://dx.doi.org/10.1074/jbc.273.1.9

Nakamura, F., M.R. Amieva, and H. Furthmayr. 1995. Phosphorylation of threonine 558 in the carboxyl-terminal actin-binding domain of moesin by thrombin activation of human platelets. *J. Biol. Chem.* 270:31377–31385. http://dx.doi.org/10.1074/jbc.270.52.31377

Nakamura, F., L. Huang, K. Pestonjamasp, E.J. Luna, and H. Furthmayr. 1999. Regulation of F-actin binding to platelet moesin in vitro by both phosphorylation of threonine 558 and polyphosphatidylinositides. *Mol. Biol. Cell*. 10:2669–2685. http://dx.doi.org/10.1091/mbc.10.8.2669

Nuckolls, G.H., C.E. Turner, and K. Burridge. 1990. Functional studies of the domains of talin. *J. Cell Biol.* 110:1635–1644. http://dx.doi.org/10.1083/jcb.110.5.1635

Nyström, M.L., G.J. Thomas, M. Stone, I.C. Mackenzie, I.R. Hart, and J.F. Marshall. 2005. Development of a quantitative method to analyse tumour cell invasion in organotypic culture. *J. Pathol.* 205:468–475. http://dx.doi.org/10.1002/path.1716

Oser, M., H. Yamaguchi, C.C. Mader, J.J. Bravo-Cordero, M. Arias, X. Chen, V. Desmarais, J. van Rheenen, A.J. Koleske, and J. Condeelis. 2009. Cortactin regulates cofilin and N-WASp activities to control the stages of invadopodium assembly and maturation. *J. Cell Biol.* 186:571–587. http://dx.doi.org/10.1083/jcb.200812176

Oser, M., C.C. Mader, H. Gil-Henn, M. Magalhaes, J.J. Bravo-Cordero, A.J. Koleske, and J. Condeelis. 2010. Specific tyrosine phosphorylation sites on cortactin regulate Nck1-dependent actin polymerization in invadopodia. *J. Cell Sci.* 123:3662–3673. http://dx.doi.org/10.1242/jcs.068163

Patsialou, A., J. Wyckoff, Y. Wang, S. Goswami, E.R. Stanley, and J.S. Condeelis. 2009. Invasion of human breast cancer cells in vivo requires both paracrine and autocrine loops involving the colony-stimulating factor-1 receptor. *Cancer Res.* 69:9498–9506. http://dx.doi.org/10.1158/0008-5472.CAN-09-1868

Patsialou, A., Y.R. Wang, J. Lin, K. Whitney, S. Goswami, P.A. Kenny, and J.S. Condeelis. 2012. Selective gene-expression profiling of migratory tumor cells in vivo predicts clinical outcome in breast cancer patients. *Breast Cancer Res.* 14:R139. http://dx.doi.org/10.1186/bcr3344

Pignatelli, J., M.C. Jones, D.P. LaLonde, and C.E. Turner. 2012a. Beta2-adaptin binds actopaxin and regulates cell spreading, migration and matrix degradation. *PLoS ONE*. 7:e46228. http://dx.doi.org/10.1371/journal.pone.0046228

Pignatelli, J., D.A. Tumbarello, R.P. Schmidt, and C.E. Turner. 2012b. Hic-5 promotes invadopodia formation and invasion during TGF-β–induced epithelial–mesenchymal transition. *J. Cell Biol.* 197:421–437. http://dx.doi.org/10.1083/jcb.201108143

Pollard, T.D. 2007. Regulation of actin filament assembly by Arp2/3 complex and formins. *Annu. Rev. Biophys. Biomol. Struct.* 36:451–477. http://dx.doi.org/10.1146/annurev.biophys.35.040405.101936

Putney, L.K., S.P. Denker, and D.L. Barber. 2002. The changing face of the Na^+/H^+ exchanger, NHE1: structure, regulation, and cellular actions. *Annu. Rev. Pharmacol. Toxicol.* 42:527–552. http://dx.doi.org/10.1146/annurev.pharmtox.42.092001.143801

Rodius, S., O. Chaloin, M. Moes, E. Schaffner-Reckinger, I. Landrieu, G. Lippens, M.H. Lin, J. Zhang, and N. Kieffer. 2008. The talin rod IBS2 α-helix interacts with the β3 integrin cytoplasmic tail membrane-proximal helix by establishing charge complementary salt bridges. *J. Biol. Chem.* 283:24212–24223. http://dx.doi.org/10.1074/jbc.M709704200

Roh-Johnson, M., J.J. Bravo-Cordero, A. Patsialou, V.P. Sharma, P. Guo, H. Liu, L. Hodgson, and J. Condeelis. 2013. Macrophage contact induces RhoA GTPase signaling to trigger tumor cell intravasation. *Oncogene*. http://dx.doi.org/10.1038/onc.2013.377

Roussos, E.T., M. Balsamo, S.K. Alford, J.B. Wyckoff, B. Gligorijevic, Y. Wang, M. Pozzuto, R. Stobezki, S. Goswami, J.E. Segall, et al. 2011. Mena invasive ($Mena^{INV}$) promotes multicellular streaming motility and transendothelial migration in a mouse model of breast cancer. *J. Cell Sci.* 124:2120–2131. http://dx.doi.org/10.1242/jcs.086231

Sakurai-Yageta, M., C. Recchi, G. Le Dez, J.B. Sibarita, L. Daviet, J. Camonis, C. D'Souza-Schorey, and P. Chavrier. 2008. The interaction of IQGAP1 with the exocyst complex is required for tumor cell invasion downstream of Cdc42 and RhoA. *J. Cell Biol.* 181:985–998. http://dx.doi.org/10.1083/jcb.200709076

Schwartz, M.A., C. Lechene, and D.E. Ingber. 1991. Insoluble fibronectin activates the Na/H antiporter by clustering and immobilizing integrin α 5 β 1, independent of cell shape. *Proc. Natl. Acad. Sci. USA*. 88:7849–7853. http://dx.doi.org/10.1073/pnas.88.17.7849

Sharma, V.P., R. Eddy, D. Entenberg, M. Kai, F.B. Gertler, and J. Condeelis. 2013a. Tks5 and SHIP2 regulate invadopodium maturation, but not initiation, in breast carcinoma cells. *Curr. Biol.* 23:2079–2089. http://dx.doi.org/10.1016/j.cub.2013.08.044

Sharma, V.P., D. Entenberg, and J. Condeelis. 2013b. High-resolution live-cell imaging and time-lapse microscopy of invadopodium dynamics and tracking analysis. *In* Adhesion Protein Protocols. Vol. 1046. A.S. Coutts, editor. Humana Press, New York. 343–357.

Shattil, S.J., C. Kim, and M.H. Ginsberg. 2010. The final steps of integrin activation: the end game. *Nat. Rev. Mol. Cell Biol.* 11:288–300. http://dx.doi.org/10.1038/nrm2871

Shimizu, R., J. Kikuchi, T. Wada, K. Ozawa, Y. Kano, and Y. Furukawa. 2010. HDAC inhibitors augment cytotoxic activity of rituximab by upregulating CD20 expression on lymphoma cells. *Leukemia*. 24:1760–1768. http://dx.doi.org/10.1038/leu.2010.157

Simonson, W.T.N., S.J. Franco, and A. Huttenlocher. 2006. Talin1 regulates TCR-mediated LFA-1 function. *J. Immunol.* 177:7707–7714. http://dx.doi.org/10.4049/jimmunol.177.11.7707

Solinet, S., K. Mahmud, S.F. Stewman, K. Ben El Kadhi, B. Decelle, L. Talje, A. Ma, B.H. Kwok, and S. Carreno. 2013. The actin-binding ERM protein Moesin binds to and stabilizes microtubules at the cell cortex. *J. Cell Biol.* 202:251–260. http://dx.doi.org/10.1083/jcb.201304052

Srivastava, J., G. Barreiro, S. Groscurth, A.R. Gingras, B.T. Goult, D.R. Critchley, M.J.S. Kelly, M.P. Jacobson, and D.L. Barber. 2008. Structural model and functional significance of pH-dependent talin-actin binding for focal adhesion remodeling. *Proc. Natl. Acad. Sci. USA*. 105:14436–14441. http://dx.doi.org/10.1073/pnas.0805163105

Steeg, P.S. 2003. Metastasis suppressors alter the signal transduction of cancer cells. *Nat. Rev. Cancer*. 3:55–63. http://dx.doi.org/10.1038/nrc967

Stylli, S.S., T.T.I. Stacey, A.M. Verhagen, S.S. Xu, I. Pass, S.A. Courtneidge, and P. Lock. 2009. Nck adaptor proteins link Tks5 to invadopodia actin regulation and ECM degradation. *J. Cell Sci.* 122:2727–2740. http://dx.doi.org/10.1242/jcs.046680

Tadokoro, S., S.J. Shattil, K. Eto, V. Tai, R.C. Liddington, J.M. de Pereda, M.H. Ginsberg, and D.A. Calderwood. 2003. Talin binding to integrin β tails: a final common step in integrin activation. *Science*. 302:103–106. http://dx.doi.org/10.1126/science.1086652

Tanentzapf, G., and N.H. Brown. 2006. An interaction between integrin and the talin FERM domain mediates integrin activation but not linkage to the cytoskeleton. *Nat. Cell Biol.* 8:601–606. http://dx.doi.org/10.1038/ncb1411

Tuomi, S., A. Mai, J. Nevo, J.O. Laine, V. Vilkki, T.J. Ohman, C.G. Gahmberg, P.J. Parker, and J. Ivaska. 2009. PKCε regulation of an α_5 integrin–ZO-1 complex controls lamellae formation in migrating cancer cells. *Sci. Signal.* 2:ra32.

Valastyan, S., and R.A. Weinberg. 2011. Tumor metastasis: molecular insights and evolving paradigms. *Cell*. 147:275–292. http://dx.doi.org/10.1016/j.cell.2011.09.024

Wang, P.B., C. Ballestrem, and C.H. Streuli. 2011. The C terminus of talin links integrins to cell cycle progression. *J. Cell Biol.* 195:499–513. http://dx.doi.org/10.1083/jcb.201104128

Webb, B.A., M. Chimenti, M.P. Jacobson, and D.L. Barber. 2011. Dysregulated pH: a perfect storm for cancer progression. *Nat. Rev. Cancer*. 11:671–677. http://dx.doi.org/10.1038/nrc3110

Wyckoff, J.B., J.G. Jones, J.S. Condeelis, and J.E. Segall. 2000. A critical step in metastasis: in vivo analysis of intravasation at the primary tumor. *Cancer Res.* 60:2504–2511.

Xing, B.D., A. Jedsadayanmata, and S.C.T. Lam. 2001. Localization of an integrin binding site to the C terminus of talin. *J. Biol. Chem.* 276:44373–44378. http://dx.doi.org/10.1074/jbc.M108587200

Yamaguchi, H., M. Lorenz, S. Kempiak, C. Sarmiento, S. Coniglio, M. Symons, J. Segall, R. Eddy, H. Miki, T. Takenawa, and J. Condeelis. 2005. Molecular mechanisms of invadopodium formation: the role of the N-WASP–Arp2/3 complex pathway and cofilin. *J. Cell Biol.* 168:441–452. http://dx.doi.org/10.1083/jcb.200407076

Yamaguchi, H., S. Yoshida, E. Muroi, N. Yoshida, M. Kawamura, Z. Kouchi, Y. Nakamura, R. Sakai, and K. Fukami. 2011. Phosphoinositide 3-kinase signaling pathway mediated by p110α regulates invadopodia formation. *J. Cell Biol.* 193:1275–1288. http://dx.doi.org/10.1083/jcb.201009126

Yan, W.H., K. Nehrke, J. Choi, and D.L. Barber. 2001. The Nck-interacting kinase (NIK) phosphorylates the Na^+-H^+ exchanger NHE1 and regulates NHE1 activation by platelet-derived growth factor. *J. Biol. Chem.* 276:31349–31356. http://dx.doi.org/10.1074/jbc.M102679200

Zhang, X., G. Jiang, Y. Cai, S.J. Monkley, D.R. Critchley, and M.P. Sheetz. 2008. Talin depletion reveals independence of initial cell spreading from integrin activation and traction. *Nat. Cell Biol.* 10:1062–1068. http://dx.doi.org/10.1038/ncb1765